EXTRACTION OF INERTIAL AND DROOP RESPONSE FROM UTILITY SCALE BATTERY PACK AT THE STATE OF CHARGING

A THESIS SUBMITTED TO THE GRADUATE DIVISION OF THE UNIVERSITY OF HAWAI‘I AT MĀNOA IN PARTIAL FULFILLMENT OF THE REQUIREMENTS FOR THE DEGREE OF

MASTER OF SCIENCE

IN

ELECTRICAL ENGINEERING

June 2018

By

Jubeyer Rahman

Thesis Committee:

Matthias Fripp, Chairperson

Reza Ghorbani

Aaron Ohta

Acknowledgments

I would like to thank those people from different schools and organizations, without whom, this thesis would not have become a reality.

I wish to express my sincere gratitude to my supervisor Dr. Matthias Fripp for hosting my thesis work in his lab, for his insightful guidance and availability at every stages of this work, and for reviewing and commenting on my final report. I also wish to extend my sincere appreciation to my thesis committee members, Dr. Reza Ghorbani and Dr. Aaron Ohta for their thoughtful comments and suggestions which, helped a lot to improve the work.

The project was partially funded by Hawaii Natural Energy Institute (HNEI). My heartiest thanks go to them.

I would also like to thank PSCAD support team for their prompt replies and solutions to many of my questions and problems while learning the software.

I wish to extend my sincere appreciation to Mr. Vasileios Karapanos of TU Delft, Netherlands for providing me the SIMULINK model of his work to start with.

Last, but not the least, I would like to thank my parents for their encouragement and sacrifice, made for me up until today.

Abstract

In weak grids, high penetration of renewable energy sources (RES) poses a major threat to the overall system stability and reliability. Absence/lack of rotational inertia worsens stability issues like frequency support in case of a disturbance. After the loss of a generating unit, fast-acting battery energy storage system (BESS) can emulate the role of the lost generator by providing the dynamic frequency support until, corrective actions are taken to restore the frequency. Unlike others, this work focuses mainly to make the BESS emulate a real generator, providing inertial and droop response at its charging state. To achieve the objective, a modification in battery charge control algorithm has been introduced. It ensures the provision of ancillary services free of cost and exclusion of any additional wear and tear on the BESS. As a test case, a customized model of a small microgrid has been used and the effect of droop and inertial response from the BESS on system's transient response, has been investigated using time domain simulations in PSCAD/EMTDC.

Table of Contents

List of Figures

List of Tables

Chapter 1

Introduction

1.1 Background

The world is seeing a dramatic change in the socio-economic condition of millions of people; most of them belong to the developing countries with fast-growing emerging economies. It has been predicted that by 2040 the world GDP will be doubled, lifting almost 2.5 billion people from low-income class to middle-income class [1]. This rise in prosperity brings about a huge increase in global energy demand, primarily contributed by the rise of energy demand in industry and transportation.
Electrification throughout the world will also continue, making power sector, accountable for 70% increase in the consumption of primary energy [1]. Up until today the majority share of this demand is satisfied by the conventional energy sources but, watershed transformation in this sector is also taking place. It is happening from the urge to bring about a decisive break to make the ever-increasing carbon emission plummet. Not only the environmental consideration or global commitments on climate change mitigation but also the development of renewable energy technology and drop in renewable energy project prices are playing a vital role in this evolution. At present more than 170 countries have some sort of renewable energy targets and around 150 countries have renewable energy supporting policies [2]. These moves have made renewable energy the fastest growing energy source, and by 2040 the world is going to have the most diversified energy mix ever happened in the history. [1].

Along with large-scale centralized power generation projects, the potential of renewable energy sources to meet the off-grid and distributed demand are gradually getting explored. In developed countries like Japan, Europe, Australia, North America, etc., the number of prosumers (residential customers who produce their own electricity through solar panels) is already on the rise. Akin to them, many developing countries are opting for decentralized, mini-grid, micro-grid and off-grid solutions to meet the demand for consumers living in remote areas since grid connection is too expensive and transmission loss is relatively high.
The evolutionary transition from conventional energy sources to renewable energy sources is not without its drawback. Since more and more traditional synchronous generators are giving their ways to RESs, it raises a serious question towards system stability. Traditionally, the system frequency is governed by the rotating speed of the synchronous generator's rotor. The rotating mass of rotor is a source of kinetic energy that helps to level any sudden difference between supply and demand and maintain system frequency within

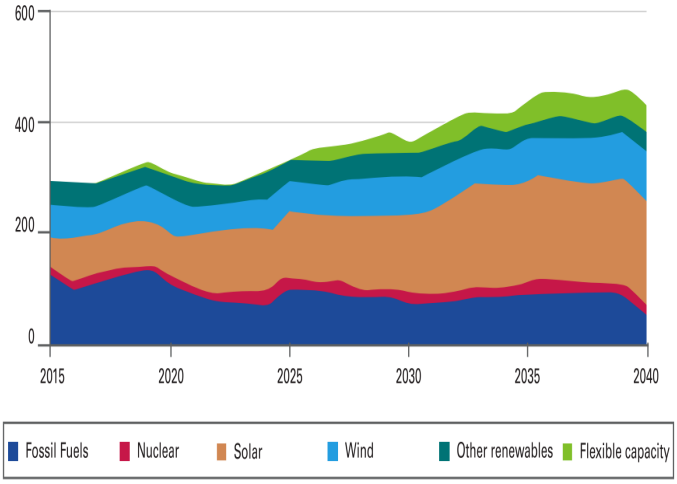

Figure 1.1: Projected global installed capacity (in GW) by resources[3]

acceptable margin either by speeding up or slowing down. This service is termed as inertial response (IR) and is a vital one to stabilize the network's performance after a disturbance.
Unlike the existence of a direct coupling between generator and grid in conventional power system, the renewable energy based generation units are usually connected to the rest of the system by power electronic inverters. It decouples the generating unit from the rest of the system resulting in a reduced or almost no control over system frequency unless otherwise some extensive modifications have been accomplished. In addition to this segregation, most of the RESs like PV don't have any rotating part which could supplement the lack of inertia phenomenon challenging the potential of RESs as a credible energy solution. This thesis focuses to use the readily available resources to deal with this stability issue without compromising system security.

1.2 Motivation

Unlike conventional technologies, the generation from RESs is not consistently available around the day, and the power output is highly variable. To tackle this inherent uncertainty in renewable energy portfolio, focus on efficient and affordable energy storage technology is increasing. ESSs can act as a buffer to system frequency fluctuation and also supplement the generation when the RESs are no longer available. Besides these, ESSs can mimic synchronous generator and provide IR along with other frequency support services. Since the power consumption of ESS is controllable, it is considered as a smart load which can effectively participate in demand-side management. With these multilateral capabilities, energy storage has become a key player in maintaining power quality and reliability in a high penetration renewable energy system.
It has been long since, the potential of ESS is being explored to provide ancillary services to system operators around the globe. In 1987 a 17 MW/14.4 MWh lead-acid battery storage system was installed in West Berlin to provide frequency support service and spinning reserve [4]. The success of this project inspired others to take on more ESS projects to solve system security concerns. Over the time, extensive research efforts

have resulted in the development of new storage techniques with longer cycle-life, more efficiency, and more maturity. Among all the available ESS technologies, BESSs have some more benefits than others. It has been reported that lithium-ion batteries are better than other ESSs in providing frequency support services [5, 6]. BESSs also win over other ESSs for their easy portability and plug and play nature. ESS technologies like pumped storage unit cannot be installed anywhere whereas, BESSs do not have such restriction. The cost of this technology has also gone down sharply in recent times; e.g., the cost of lithium-ion modules has decreased more than 70 percent since 2012 [7]. Considering these characteristics, BESS get a clear advantage over others, when it is proposed to be installed within an isolated grid or micro-grid at remote areas.
Most of the research work so far, have focused to harness the potential of BESS for frequency support services at its discharging state leaving its potential, at charging state, mostly unexplored. It is an area worthy of being sought for since, at this state, frequency services can be achieved free of cost without putting any extra wear and tear on BESS.

1.3 Objectives

1.3.1 Main Objective

The primary target of this work is to investigate the potential of a lithium-ion based BESS to provide inertial response and droop response services to a micro-grid at its charging state.

1.3.2 Specific Objectives

The following targets are meant to be done to achieve the ultimate goal of this work.

- Develop customized models of micro-grid for simulation based on different requirements for different study cases.
- Study and develop control schemes for grid interfacing converters according to specific system requirements.
- Develop control schemes for diesel generators present in the proposed micro-grid model.
- Review existing methods for IR and droop response emulation and develop appropriate power electronic control schemes to control the charging current for providing IR and droop response from BESS.
- Evaluate the performance of the proposed control schemes at different study cases and compare with the results of other work performed at discharging state of BESS available so far.

1.4 Methodology

To start with, a comprehensive review has been accomplished on the research work that has been done so far in this field. Then a simulation environment is created in PSCAD. PSCAD is a well known EMTDC simulation engine with a handy graphical user interface. The reason for choosing PSCAD is, its ability to simulate the dynamics of power system when the electromagnetic transient response takes place right after

a fault situation. It turns out even better than other software available at hand when it comes to design the speed governor control system of the synchronous generators present in the system. To compare and evaluate the proposed control algorithm, mainly two types of customized model have been prepared. One contains only four diesel generators and a linear load; other has two diesel generators, a PV farm, a linear load, and a Li-ion BESS. First of all, a system resembling the traditional power system with only four diesel generators and a linear load has been modeled. It gives the frequency response that is supposed to occur in a conventional power system after a fault takes place. Here the generator rotors and speed-governors are contributing to restore the system frequency to a steady state. In the next stage, two of the generators have been taken out from the system and is replaced by a PV farm and a Li-ion BESS. Modifications have been done in the charging control topology to see whether the BESS can emulate the behavior of synchronous generators in the time of a system fault or not when it is at its charging stage. Different study cases have been arranged for that purpose; one, having only droop control algorithm activated and the other has both droop and inertial response in action. The results obtained from different study cases have been compared with each other regarding different performance indices.

1.5 Shortcomings

While doing this work several things have been ignored due to time and technical constraints and some assumptions have been made to keep the model simple. Further work can be done to eliminate these shortcomings and make the work more rigorous. Among all of them, a few are as follows:

a) The conducted simulation is not a real-time simulation. So, it doesn't show all the characteristics of the real-time frequency response of the system.

b) In the used battery model, the peukert[8] effect has been ignored which means the magnitude of the charging current doesn't affect the battery capacity.

c) Optimal sizing of BESS has not been accomplished.

d) Reactive power control hasn't been dealt that rigorously, and is beyond the scope of this work.

e) The damping effect[9] supposed to be present during the transient to attenuate the oscillation, has not been taken into account.

f) Optimal inertia emulation[9] has not been adopted.

g) Full range of frequency support has not been studied. Secondary and tertiary frequency control schemes have been excluded from the scope.

h) A linear model has been picked up for the load. So, the work doesn't study the effect of non-linear loads on system dynamics.

i) The PV farm model used here, is made as a constant real power generating unit. Change in irradiance or shading effect has not been studied.

j) The charging mode and discharging modes are chosen manually. There is no automatic control scheme for that.

k) Some of the filter parameters and constant coefficients for controllers have been set by trial and error.

1.6 Thesis Outline

This thesis contains five chapters. Chapter 1 discusses the background and motivation for this work. It also sheds some light on the aim and method of performing the work. Some limitations accompany the aforementioned items, suggesting the area of improvement. Chapter 2 contains some information about the previous work people have done so far, in this area. Existing approaches to avail the frequency response from ESS are discussed. Along with these, mechanisms or stages of frequency response and importance of inertia have been described very briefly. The whole system design has been discussed in chapter three. It has the design details of diesel generator governor control, grid side filters, VSC control, and battery charge controller. Chapter 4 discusses the study cases and results obtained from the simulation of them. Chapter 5 has the conclusion and discussion on the probable expansion of this work.

Chapter 2

Literature Review

2.1 Overview of Frequency Response

Generally, in a power system, the total electricity generation must be consumed up instantly. If whatever produced, cannot be consumed, it will be wasted anyway. That's why the balance between generation and demand is always very important for the sake of system's efficiency and stability. The frequency of a system is an important parameter that tells about whether the system has equilibrium between power production and consumption or not. Typically there is a nominal system frequency or frequency set point; from which the deviation is observed when there is a mismatch between active power production and demand. Usually, the response of a power system to the outage of large generation or load, regarding frequency can be classified into several control stages. The criteria for this classification lie in the difference in the mechanisms to provide frequency support services and in the difference in operating time scales. The following figure illustrates different regimes of comprehensive frequency control of a power system.

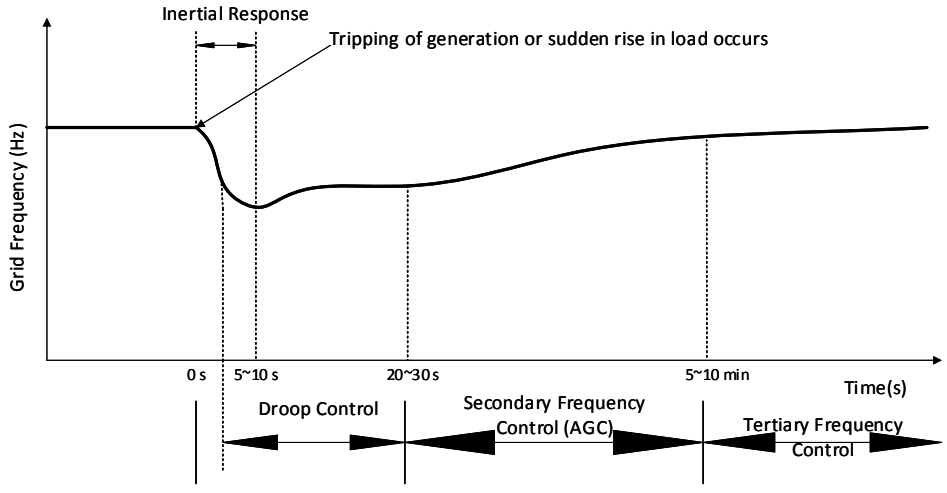

Figure 2.1: Typical system frequency response to a generation outage or sudden load change[10]

From the above figure it can be seen that there are four stages of frequency response which are,

- **Inertial Response:** From the inertia of the rotating masses present in the system
- **Droop Response or Primary Frequency Control:** From turbine governors of the synchronous generators
- **Secondary Frequency Response or AGC:** From output power control scheme in response to the system operator's power demand
- **Tertiary Frequency Response:** From manual changes in the dispatching of generating units.

Though not in the list but, there is another stage called 'electromagnetic stage'[11] that takes place before IR kicks in. Immediately after the disturbance, due to rotational inertia, the rotor angle cannot change, resulting in an impediment to the release of stored kinetic energy in the rotating mass of the rotor. In this case, the energy comes from the stator magnetic field of the synchronous machine[12]. This inherent type of response lasts around one-third of a second[13]. In the coming sections every other stage will be discussed in details; out of them IR and droop response have been emphasized, as they are the main focus of this work.

2.1.1 Inertial Response (IR)

In a conventional power system, synchronous machines(generators) converts mechanical energy to electrical energy. There are prime movers (mainly engines or turbines) which drive the rotors of synchronous machines. The generator's rotor is a rotating mass which gets kinetic energy accumulated while being rotated. The active power output from a synchronous generator is governed by a governor, which operates on a power-frequency droop characteristic[13]. The rotating mass of the rotor contributes to the active power output of the generator. In addition to that, it adds inertia property to the power line frequency through the release of stored kinetic energy at times of disturbances. Figure 2.2 shows the fundamental dynamics of electricity generation at the production end.

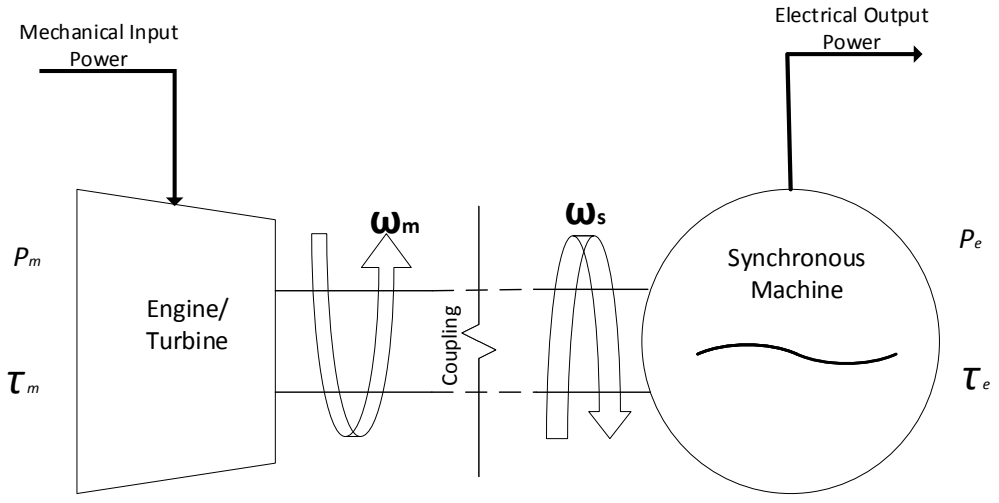

Figure 2.2: Dynamics of the prime mover and synchronous machine

In terms of mathematical representation, the rotor dynamics of the synchronous generator can be described as follows:

$$\tau_m - \tau_e = J\alpha \tag{2.1}$$

$$\tau_m - \tau_e = J\frac{d\omega_m}{dt} \tag{2.2}$$

Where,

α [rad/s^2] =Angular retardation or acceleration of the rotor
ω_m [rad/s]= Synchronous angular velocity of the rotor
J [kg.m^2]= Moment of inertia of the rotor
τ_m [N.m]= Mechanical torque exerted by the prime mover
τ_e [N.m]= Electromagnetic torque exerted by the system load

Equation 2.2 is known as the 'Swing Equation' in power system. But it is customary to represent the equation in terms of real power, instead of torques. By using the relation $P = \tau\omega$, (P is the active power) the aforementioned equation takes the following form:

$$P_m - P_e = J\omega_m\frac{d\omega_m}{dt} \tag{2.3}$$

Where,

P_m [W]= Mechanical power input
P_e [W]= Electrical power output

When there is an imbalance between the mechanical power output from the generation side and electrical load demand from the consumer side, the rotor either speeds up or slows down (depending on the type of disturbances) to offset the power mismatch. This type of response which is kind of inherent to every synchronous machine, present in the system, is termed as inertial response (IR). This mechanism can better be understood by the following relation between stored kinetic energy and real power mismatch.

$$P_m - P_e = \frac{d(E_k)}{dt} \tag{2.4}$$

Where,

E_k [J]= Stored kinetic energy in the rotor

This stored kinetic energy is directly related to the inertia of the rotor.

$$E_k = \frac{1}{2}J\omega_s^2 \tag{2.5}$$

Where,

ω_s [rad/s]= Synchronous electrical radian frequency

The variation in rotor speed is reflected electrically by a change in network frequency. To be specific, the system frequency changes at a certain rate which is governed by the cumulative inertia of all spinning generators and composite damping from rotating loads like induction motors etc.[14, 15, 16] . However, in this work, the composite damping effect from rotating loads is ignored.

There is an important parameter called inertia constant ($H[s]$), whose understanding is central to quantify

the rotating masses of the system. It can be defined as,

$$H = \frac{E_k}{S_{base}} = \frac{\frac{1}{2}J\omega_s^2}{S_{base}} \tag{2.6}$$

Where,

S_{base} [VA]= Base apparent power of the system

By substituting the expression of J obtained from equation 2.6 to equation 2.3 yields,

$$P_m - P_e = \frac{2HS_{base}}{\omega_s^2}\omega_m \frac{d\omega_m}{dt} \tag{2.7}$$

If there exists more than one synchronous machine and if they are in phase with each other, equation 2.7 can still be used as an aggregated single mass model[17]. By observing the above equations and the classical definition of inertia in mechanics, inertia in the conventional electrical power system can be defined as the opposition to the transformation of stored kinetic energy in rotating masses to counteract the frequency deviation from nominal value after a disturbance. The higher the total inertia present in a system, the slower the rate of change of frequency (ROCOF) will be. In fact, systems with high rotational inertia have more time to support the system frequency to remain within acceptable bounds before the next stage of frequency response; droop response comes into action. In agreement with the definition just given, a new form of equation 2.7, shows the relation between the active power mismatch and ROCOF of the power network as follows:

$$P_m - P_e = \ K_d \frac{df}{dt} \tag{2.8}$$

Where,

K_d [W.s^2]= Inertia coefficient

The total kinetic energy which is transformed during a fault situation can be described as:

$$\int (P_m - P_e)dt = \sum \Delta E_k \tag{2.9}$$

Usually, IR remains there only for a few seconds. If no further steps are adopted to correct the frequency deviation, it will not be able to hold the system for too long. At one point, the kinetic energy will get all used up, and the system will collapse.

2.1.2 Droop Response or Primary Frequency Control

Droop response or primary frequency control service is mainly provided by the governors of synchronous machines. Usually, governor maintains the balance between mechanical power(P_m) and electrical output power (P_e). When the balance is disturbed, the governor realizes it through feedback from the rotor speed (ω_m). When the rotor slows down, (a decrease in ω_m)that means P_e becomes higher than P_m, the reference power level is increased; to respond to that the governor arranges to increase P_m, by either allowing more steam or water to hit the turbine or by increasing the fuel supply to engines which in turn increases the rotational speed of the prime mover. It works in the opposite way when the reverse things happen; if P_m

becomes greater than P_e the rotor speeds up(ω_m increases), to slow it down, governor manages to reduce the speed of prime mover or turbine. The effect of rotor speed either slowing down or speeding up is directly reflected in power network's frequency (f). In terms of system level realization, if frequency deviates from its nominal value that means generation is more or less than the required amount, the existing generators in the system increases or decreases their output to share the load/demand variations proportional to their governors' droop setting. The conventional equation for a generator governor's droop response looks like the following:

$$P_{ref} - P = K_p(f_{ref} - f) \tag{2.10}$$

Where,

K_p [kW/Hz]= Droop coefficient

f_{ref} [Hz] = Nominal value of the system frequency

P_{ref}[kW]= Nominal active power output

P [kW]= Active mechanical power output

In accordance with equation 2.10, the droop curve looks like the following.

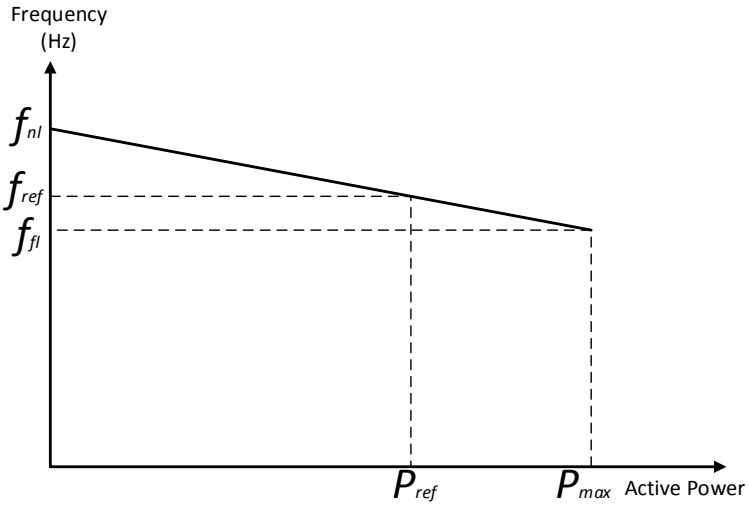

Figure 2.3: Active power frequency relation of a governor

Here, f_{nl} is the no-load frequency in Hz, f_{fl} is the full-load frequency in Hz and P_{max} is the maximum active power that a synchronous generator can provide. The droop coefficient K_p is denoting the rate of this operation curve.

There are different types of droop control like $P-f$ and $Q-V$ droop control,$P-V$ and $Q-f$ droop control, etc. The choice is made on the output impedance of the system [18, 19, 20]. In this work, $P-f$ droop has been performed as the output impedance is mainly inductive here [21].

A reserve of active power is kept standby to provide droop response which is called primary frequency control reserve. This reserve has got two different names depending upon the situation at which, it is being applied. Positive frequency control reserve supplements whenever frequency experiences a downward movement and negative frequency control reserve acts to handle upward movement in frequency. The main advantages

of droop control are, it is local and automatic and doesn't require any external communication link. The time frame for droop control ranges from seconds to 20/30 seconds after the disturbance. But droop control doesn't provide the full package of frequency control. The governor's droop response helps to bring the frequency at a steady state level but not to the nominal setpoint. There remains a certain amount of difference between the new steady state value and original system set point which, is corrected in the later stages of frequency response.

2.1.3 Secondary Frequency Response or Automatic Generation Control (AGC)

The steady state frequency error is corrected in secondary frequency control stage. That's why it is termed as the recovery stage at times. This is a centralized control where the system operator sends correcting commands to generating units to adjust their active power output set points. When the active power set points are changed, it brings back the system frequency and net tie-line power flow across areas to their reference values. Secondary frequency control is more area-specific whereas, each area should take care of maintaining its generation-load balance. Though not utilized in all types of power systems (e.g., Great Britain[22], some isolated power systems[24]), secondary frequency control is used extensively in all large interconnected systems[22] due to the inability of manual control to eliminate overload situation quickly on tie lines between neighboring areas. Usually, secondary frequency control comes into action in around minutes after the disturbance takes place and performs its action within 5-10 minutes.
The mechanism by which secondary frequency control or AGC works is mainly based on the deployment of secondary control reserve to minimize 'Area Control Error (ACE)' [23], defined in the following equation:

$$ACE = (P_{cross-area} - P_{cross-area,ref}) + \beta(f - f_{ref}) \tag{2.11}$$

Where,

$P_{cross-area}$ [kW]= Active power exchange between interconnected areas
$P_{cross-area,ref}$ [kW] = Reference value of cross-border power exchange
β [kW/Hz] = Frequency bias constant

Change in reference power set-point of each generator's speed-governor, participating in the secondary frequency control scheme, can be related to the ACE like the following:

$$\Delta P_{ref} = -K_i \int ACE.dt \tag{2.12}$$

ΔP_{ref} [kW]= Change in reference active power setting
K_i = Integral gain, constant

The monitoring of ACE parameters and computation of ACE are performed separately for each area. Then the system operator sends either raise or lower commands to each participating speed-governors based on the calculation according to equation 2.12 from measured ACE. For example, if either the net cross-border power flow out of an area or the area frequency becomes less than the reference value, then ACE becomes

negative and the change in reference power (ΔP_{ref}) becomes positive; it makes the system operator send commands to all generating units in that area to raise their generation.
The speed of secondary frequency response to bring the system frequency back to the reference value depends on the magnitude of the error. The process of recovering the frequency should be finished before the full depletion of primary frequency reserve takes place. Actually, the operation time-frame of primary frequency control and secondary frequency control have some common time horizon, and the generation-load balance is recovered by primary frequency control[22].

2.1.4 Tertiary Frequency Control

Tertiary frequency control either works in succession or as a supplement to secondary frequency control. It frees up primary and secondary frequency control reserves, brings back the cross-border power exchange and system frequency to their reference values when the secondary frequency control scheme fails to do so. Trading of energy sometimes also belongs to tertiary control scheme to maintain generation-demand balance. It performs the change in unit commitment and dispatching of generating units through manual control. Its operation time-frame ranges from tens of minutes up to hours.

2.2 Emulation of Inertia: A Review of Available Sources

The low-inertia, resulting from the phasing out of conventional generating units in favor of power electronic converter based energy sources, is not well-equipped to tackle the frequency excursions at upsets of electric power mismatch. Among many attempts made to address reduced inertia problem, inertia emulation has taken a significant amount of research efforts. The main trait of 'virtual inertia emulation' is to imitate the effect of rotational inertia usually available from conventional synchronous machines on the power grid. A plethora of schemes have been developed to mimic the rotational inertia from non-synchronous sources. Efforts have been made to provide IR from wind turbines [25], flywheels [26],pumped hydros [27], VSC-HVDC systems [28], different types of capacitors [24], batteries[29] etc. In the coming sections, the usage of some of the aforementioned technology in providing IR will be reviewed.

2.2.1 Inertia Emulation from PV

PV systems are devoid of rotating parts, thus unable to provide inertia directly. It can only store a small amount of energy in the dc-link capacitor to be deployed at the power electronic interface with the grid. But PV systems can provide inertia by de-loading[30, 31]. In that scheme, the PV system operates at a sub-optimal point to keep the power reserve available to provide inertial response. The control loop is implemented at DC-DC converter side that makes the PV unit inject or absorb extra power when there is a deviation in system frequency. From technical point of view, it is not a very alluring solution due to the inefficient use of generating units. It incurs a lot of energy waste, as the system always has to run below its maximum capacity to ensure the availability of sufficient energy reserve for fault situation. Extra power electronic elements for implementing the control loops often put this solution down the line for their high expenses. Besides all these drawbacks, the scheme has some benefits as well. In [32], de-loading PV scheme has been proved to be more economical than using the battery in dynamic frequency support service.

2.2.2 Inertia Emulation from Wind Power Plant

Unlike PV, there exists turbine which is a rotating mass and has rotational inertia. Depending on the wind turbine topology, the capability of providing IR varies. Fixed speed wind turbines that use 'Squirrel-Cage Induction Generator' and limited variable speed wind turbines that use 'Wound Rotor Induction Generator' are coupled to the electrical grid via transformer, can provide IR [33]. But as the input wind speed doesn't remain consistent all the day, there are turbine topologies that use power electronic converters which decouple the turbine from the grid. In those cases, the wind turbines have limited or no capability to provide inertial response unless some additional controllers are added to the system. The mechanism to extract inertial response from converter interfaced wind power plant is pretty much similar to that of from PV. The wind turbine acts as a current source, and the output power from the turbine is controlled by an MPPT. After incorporating a derivative term of the system frequency, the swing equation, representing the output of the turbine, can be derived like the following[34].

$$P_{out} = P_{MPPT} - M\frac{df}{dt} \tag{2.13}$$

P_{out} [kW]= Active power output of the wind turbine
M [kW.s^2]= Derivative inertia constant

The second term in the above equation supplements the active power mismatch between production and demand and thus supplies the inertial response. Incorporation of that term in swing equation yields a new reference power set point for MPPT. It is possible to extract more energy than the physical stored energy in turbine as long as the extraction does not take the turbine out of its operating range or make it stalled[35].

2.2.3 Inertial Response from both Synchronous Generators and ESS

In most of the microgrids, the power system is composed of renewable energy sources (RESs), energy storage systems (ESSs) and synchronous generators. The solution for reduced inertia problem is sought among the existing components in the system. In most of the cases, the performance of the whole system is judged based on the nature of the response from the system. Usually, it is the concerted effort of energy storage system and synchronous generator that helps to keep the system in balance after a contingency takes place. Specially, energy storage system also contributes to balance the fluctuation in power generation from renewable energy sources which are highly stochastic . So, the power generation in total from both synchronous generator, RESs and energy storage should match with the total demand.

$$P_{SM} + P_{ESS} + P_{RES} = P_{load} \tag{2.14}$$

Where,

P_{SM} [kW]= Active power output of the synchronous generators
P_{ESS} [kW]= Active power output from the energy storage system
P_{RES} [kW]= Power output from renewable energy sources
P_{load} [kW]= Total load demand

Almost all the work done so far [24, 34, 36, 37, 38, 39], have demonstrated the improvement in frequency response when energy storage systems are providing inertial response by injecting power to the system to-

gether with synchronous machines. So, the total inertial response is the sum of inherent inertial response from synchronous machines and the injected inertia from energy storage system. The aforementioned references have shown that along with the synchronous machines in the system the ESSs help to improve the frequency nadir and frequency settling point and time it takes to reach the steady state when ESSs output is controlled to yield power, proportional to the negative of the derivative of the rotor speed.

2.3 Virtual Inertia Emulation: Topologies

Among the schemes which are most commonly used for emulating virtual inertia are 'Virtual Synchronous Generator (VSG)', 'Synchronverter', 'Virtual Synchronous Machine (VISMA)' etc. More or less they are developed based on the idea that, inverters will mimic synchronous rotating machines. But there exist some differences in their methodologies.VISMA technique is established by using some real-time measurements of electromagnetic synchronous machine parameters[40]. The voltages at the 'Point of Common Coupling (PCC)' are measured and, from there, the corresponding phase currents are obtained. They are used as references to control the inverter to mimic the behavior of a synchronous machine. In 'Synchronverter', the phase currents are measured, and the output voltages of the inverter are calculated. These output voltages resemble the back emf, supposed to be supplied by a conventional synchronous machine under the same condition[41]. VSG technique is all about inverters, mimicking rotational inertia of synchronous generators. It doesn't incorporate the other parameters of synchronous machines[42].

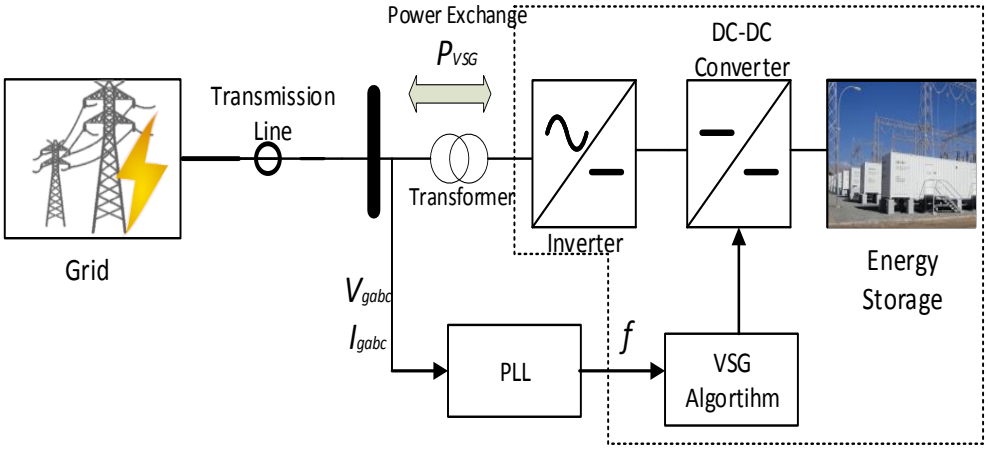

Figure 2.4: Block diagram of VSG concept: Area encircled by broken line represents VSG structure

A VSG is composed of an energy storage device, a power processor and, a controller that implements the VSG control algorithm [43].

It is expected that the VSG will emulate characteristics that will provide frequency support services especially inertial and droop control; the desired power output from VSG can be synthesized by combining equation 2.8 and 2.10.

$$P_{VSG} = K_p(f_{ref} - f) + K_d\frac{df}{dt} \tag{2.15}$$

Among all the available topologies, the VSG topology has been used in this work for its simplicity. Though

the fundamental principle of all inertia emulation topologies is pretty much same, there exist some differences in their detailed mechanisms as well. Four most widespread subcategories of these topologies will be discussed in following subsections.

2.3.1 VSG Topology from 'VSYNC' Project

One of the topologies of VSG was proposed and developed under 'VSYNC', funded by European Commission. It stands for 'Virtual Synchronous Machines for Frequency Stabilization in Future Grids with a Significant Share of Decentralized Generation'. Depending on the size the VSG is classified into two types[43];

- Small-size VSG: Used in single phase for low-voltage, low-power application.
- Medium-size VSG: Used in three phase system.

Both types of the systems have pretty much same structure, and their working principles are also the same. The control structure is composed of two levels; high and low. In low-level control, the IGBT's switching, current/voltage measurements, etc. are done. The park transformation of phase voltages and currents to the d-q components in the synchronous reference frame is done at this level. The reference frame is defined by the phase angle θ which is measured by a component called 'Phase-Locked Loop (PLL)'. The high-level control calculates the amount of real and reactive power, supposed to be provided by VSG. System frequency and phase voltages in the d-q reference frame are fed as inputs to high-level control. A signal generated from the energy management system and carrying the information about the 'State-of-Charge (SOC)' of the energy storage or battery is also fed to the high- level control block. The high-level control unit is responsible for controlling the power exchange between dc side and ac side.

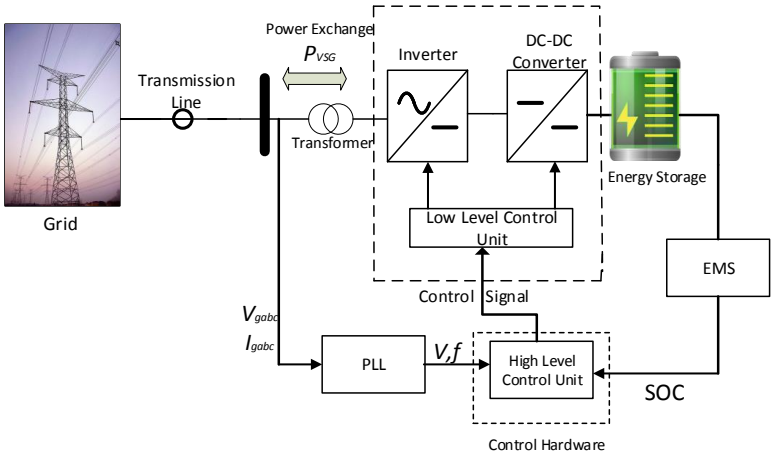

Figure 2.5: VSG structure from 'VSYNC' project based on [42]

The amount of power exchange to and from VSG is given by the following equation,

$$P_{VSG} = K_{SOC} + K_p(f_{ref} - f) + K_d\frac{df}{dt} \tag{2.16}$$

$$Q_{VSG} = K_v(V - V_{ref}) \tag{2.17}$$

Where,

K_{SOC} [kW]= Active charge-discharge power of the energy storage

K_v [Var/V]= Voltage controller gain

V_{ref} [V]= Reference voltage

V [V]= Measured voltage

2.3.2 Virtual Synchronous Machine with Hysteresis Controlled Inverter

Virtual Synchronous Machine (VISMA), proposed in[44], emulates virtual torque, virtual excitation and a virtual rotating mass, thus provides a broad range of dynamic and static property compound of a synchronous machine. The VISMA is based on a fast current control method. To implement that, information about grid voltage(V_{gabc}) is acquired and fed to a virtual synchronous machine algorithm which includes almost all the static and dynamic properties of an electro-mechanical synchronous machine model. The model includes mathematical description of a stator circuit and mechanical subsystem. The damping feature and rotating mass effects are obtained from them. Reference currents(I_{ref}) are generated from the model as output. These reference currents go into a hysteresis controller which controls a fast inverter through PWM signals. Figure 2.6 shows the major components in the fast inverter based VISMA.

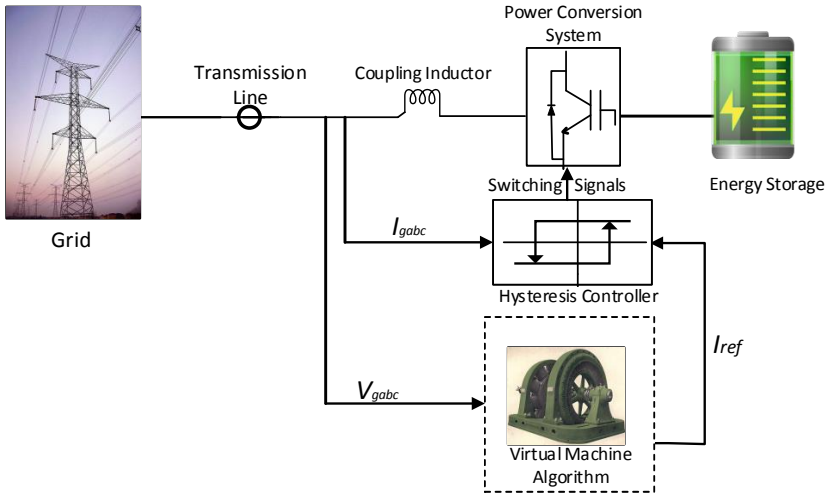

Figure 2.6: VISMA Structure

The reference current input to hysteresis controller is calculated in laplace domain as per the following equation.

$$I_{ref}(s) = \frac{E(s) - V_{gabc}(s)}{R_s + s.L_s} \tag{2.18}$$

Where,

E [V]= Induced emf in the stator winding

R_s [Ω] = $Stator - resistance$

L_s [H]= Stator inductance

Two parameters are central in the VISMA algorithm; one is the mechanical power output of the model, and another is the induced emf (E). The mechanical power output from the VISMA algorithm dictates the active power output from the energy storage, and electromotive force in the algorithm is responsible for controlling the grid voltage. The dynamics of the virtual rotor, supposed to be mimicked by the VISMA can be expressed like the following swing equation, and mechanical output power can be easily calculated henceforth.

$$\tau_m - \tau_e = \frac{1}{J}\frac{d\omega}{dt} + k_d\Delta\omega \tag{2.19}$$

Where,

ω [rad/s]= Angular velocity
J [kg.m^2]= Moment of inertia
τ_m [N.m]= Mechanical torque
τ_e [N.m]= Electrical torque
k_d [N.m.s/rad]= Mechanical damping factor

Induced emf in the stator winding can be calculated through the incorporation of rotation angle ($\theta = \omega t$) and an adjustable voltage amplitude (E_p).

$$E = \begin{bmatrix} E_1 \\ E_2 \\ E_3 \end{bmatrix} = E_p \begin{bmatrix} sin(\theta) \\ sin(\theta - \frac{2\pi}{3}) \\ sin(\theta + \frac{2\pi}{3}) \end{bmatrix} \tag{2.20}$$

2.3.3 VSG with Voltage Ride-Through Capability

VSG topology with voltage ride-through capability was proposed by [45]. It is based on the swing equation similar to that of equation 2.3, but it also takes the damping effect into account. So, the central governing equation of this topology looks like,

$$P_{in} - P_{out} = J\omega_m\frac{d\omega_m}{dt} - D.S \tag{2.21}$$

Where,

D [kW]= Damping factor
S [-]= Slip

Virtual mechanical phase ω_m is calculated from aforementioned swing equation. It is integrated and fed into the inverter controller as phase command. There is another input to the controller which is the reference voltage, calculated by a PI controller. In this topology, input power P_{in} is also set as an input. Three control schemes have been proposed under this topology to offer voltage ride-through capability.

- Voltage amplitude control for overcurrent suppression: Overcurrent phenomenon occurs when there exists a mismatch between grid voltage and inverter output voltage. To suppress that overcurrent,

inverter output voltage is synchronized with the grid voltage thus, taking the current magnitude at a minimum level.

- Power control for overcurrent suppression: The power command input to VSG algorithm is usually kept constant. If it is kept constant even at the event of a voltage dip, then overcurrent phenomenon will occur. The reason is, a drop in output voltage results in a drop of the output power. So, input power command needs to be adjusted to avoid the overcurrent event.
- Virtual resistance control: How long the unbalanced overcurrent will sustain, depends on the resistance and reactance between grid and inverter. Specifically, it is the value of the resistance that determines how long or how short the time constant for oscillation will be. If the resistance is high then the time constant will become small, and the oscillation will die out quickly and overcurrent will get reduced fast. In order to get a shorter time constant, a virtual resistance is added to the controller algorithm.

The schemes discussed above have been illustrated in the following figure where voltage amplitude control is shown in block A, power control in block B and virtual resistance control in block C. Here, P^*_{out} denotes reference output power.

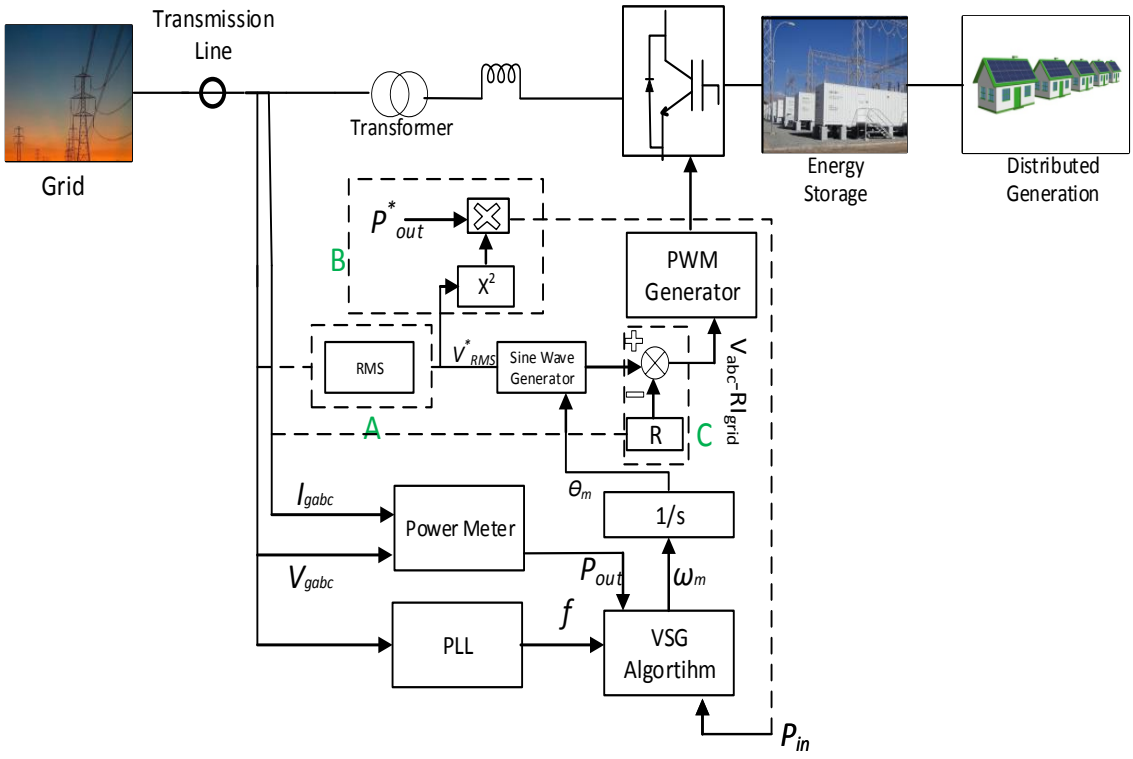

Figure 2.7: Schematic of VSG with VRT capability

2.3.4 Algebraic type VSG

The algebraic model of VSG[46] mainly addresses two issues, the low output impedance of inverters and reduced inertia of power electronic converter /inverter based system. To mimic the behavior of real syn-

chronous generator, a phasor diagram [47, 48] has been used to implement the virtual synchronous generator algorithm, and a current-controlled inverter scheme has been adopted. In addition to that, a control system has been proposed to imitate the AVR response of real generator. Altogether they offer frequency control, power factor control and voltage control just like a conventional generator. This scheme specifically offers very satisfactory operation in dealing with non-linear and unbalanced loads. Following figure gives a bit details about this scheme. Here, E_f denotes generator's internal emf, and V_g stands for its terminal voltage. R and X denote synchronous reactance and armature resistance of the model.

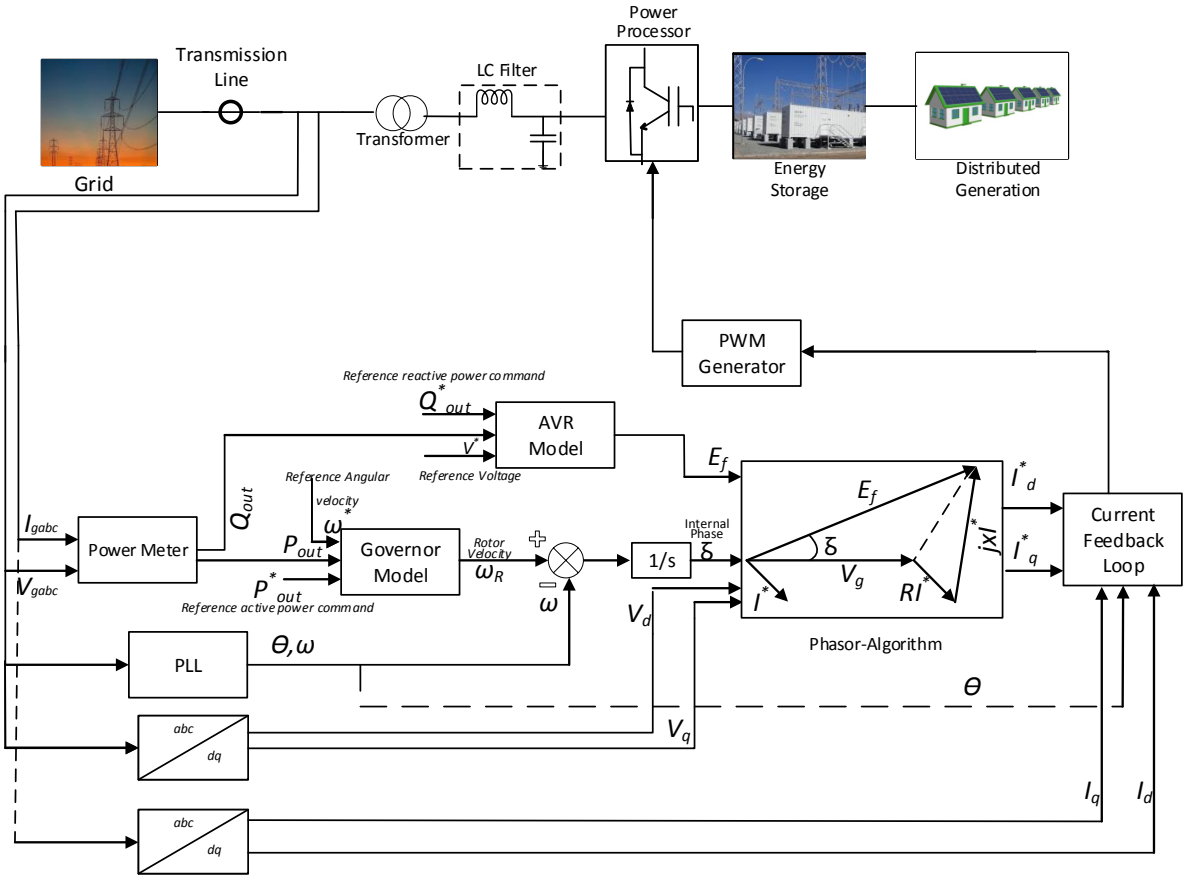

Figure 2.8: Algebraic VSG Concept

The control signal for the current controlled inverter is generated by the current feedback loop which takes the direct(I_d) and quadrature axis current (I_q) components of the grid and armature currents $I^*{}_d$ and $I^*{}_q$ as input. The grid components are achieved by performing park transformation, and armature currents are obtained by the following operation on internal emf and terminal voltage components.

$$\begin{bmatrix} {I^*}_d \\ {I^*}_q \end{bmatrix} = Y\Big(\begin{bmatrix} E_d \\ E_q \end{bmatrix} - \begin{bmatrix} V_d \\ V_q \end{bmatrix} \Big) \tag{2.22}$$

Where,

$$Y = \frac{1}{R^2 + X^2} \begin{bmatrix} R & X \\ -X & R \end{bmatrix} = \begin{bmatrix} Y_{dd} & Y_{dq} \\ -Y_{dq} & Y_{dd} \end{bmatrix} and, \begin{bmatrix} E_d \\ E_q \end{bmatrix} = E_f \begin{bmatrix} cos(\delta) \\ sin(\delta) \end{bmatrix}$$

2.4 Energy Storage System(ESS)

As energy storage system is central to the virtual synchronous generator, it is very important to choose the best one among the available technologies. As this work not only focuses on inertial response but also on primary frequency response, the capability to support both should be taken into consideration. Hence, response time and energy density are considered as the most important selection criteria. In this section, different energy storage technologies from the perspective of frequency support services will be discussed briefly, followed by the discussion on the reason for preferring BESS over others. As the focus is on converter/inverter dominated small power system, technologies related to that specific category will be discussed.

2.4.1 Hydrogen Storage

Though promising but the technology of hydrogen storage hasn't yet reached its maturity. Currently, two approaches are proved to be somewhat viable to store energy by using this technology. One is pressurized hydrogen technology, and the other one is adsorption in metal hydrides.

In pressurized hydrogen approach, hydrogen gas is stored in a high- pressure container. Depending upon at how much pressure the container can store hydrogen determines how much hydrogen can be stored per unit weight. The more the pressure higher the ratio of hydrogen storage per unit weight. This fact clips the capacity of hydrogen storage at some point as, materials which can sustain that much pressure consistently is either expensive or scarce.

For storing and using hydrogen via adsorption technology, metal hydrides are chosen for their excellent hydrogen absorption properties[49]. They have low equilibrium pressure at room temperature thus proving them safe. In addition to that, they are pretty efficient in terms of storage capacity as they have high volume absorption capacity. Though it has many merits, it is quite expensive. It requires expensive thermal management system as it emits heat when hydrogen is absorbed to this material (exothermic reaction), and it absorbs heat when hydrogen is released (endothermic reaction).

The main demerit of all the available hydrogen storage technology is related to the main component of it; hydrogen. It is required a significant amount of electrical energy to extract hydrogen from water through electrolysis. In fact, the high expense is deterring the technology from being deployed in massive scale. It has been reported by DOE that, currently 21 MW installed capacity belongs to hydrogen storage technology

around the world[50].

2.4.2 Supercapacitors or Ultracapacitors

Supercapacitors are just like the regular capacitor except the capacitance is very high from the same sized package. Molecular thin-layered electrolyte is used as the dielectric medium. Usually, static charges are used for storing energy. The properties responsible for producing large capacitance, are larger surface area of the electrodes and much thinner electrical layer between electrode and electrolyte.
Super-capacitors are pretty fast to respond to frequency disturbances in the grid. They are able to absorb and supply large bursts of power[51] but they have low energy density. In addition to that, they are more expensive than some of the battery technologies. Super-capacitor may be a good choice where a high amount of energy is not necessarily required but only response time matters.

2.4.3 Battery Energy Storage

The recent development in battery technology has cut down its cost significantly and allows people to use it for various grid services including frequency support services. Unlike super-capacitors, it has higher energy density and is less expensive. It is more efficient in terms of capacity and efficiency in storing energy. Systems which has PVs in them, require the excess energy produced at daytime to be stored for future use, can find battery energy storage more suitable than any other. Power electronic converter based battery energy storage units can be deployed very fast if required(in the scale of a few ms)[39]. Batteries are easily portable, don't require any particular geographic pattern and suited very well to be used in hybrid energy storage system with other storage devices as well.
Usually for grid support services, three types of batteries are used, namely, lead-acid batteries, Ni-based batteries and, Li-based batteries. A comparison among them based on different performance criteria is presented in the following table.

Parameter	Pb-acid battery	Ni-Cd	Li-ion
Life (in years of service)	3-12	15-20	10-20
Life (in cycles)	<1500	<3000	1000-3000
Tolerance of overcharge and deep discharge	very low	low	low
Energy density	30 Wh/kg	15-50 Wh/kg	80-150 Wh/kg
Power density	180 W/kg	50-1000 W/kg	500-2000 W/kg
Energy efficiency	85-90%	60-83%	85-90%
Self discharge rate/month	2%	10%	<5%
Price/kWh	50-100$	400-2400$	$900-1300[1]

Table 2.1: Comparison among battery parameters, typically used as energy storage[49, 52]

Though cost plays a vital role in influencing the decision for choosing one, little more expensive technology sometimes outperform cheaper options regarding specific requirements. As per the requirement of this work, it is needed to provide or absorb high amount of power pretty quickly to maintain the system equilibrium,

power density and energy density are the main points to look at for deciding which one to pick up. So, Li-ion batteries are preferred than any other available technologies in this regard. The figure below shows a comparison among different battery technology in terms of gravimetric power and energy density.

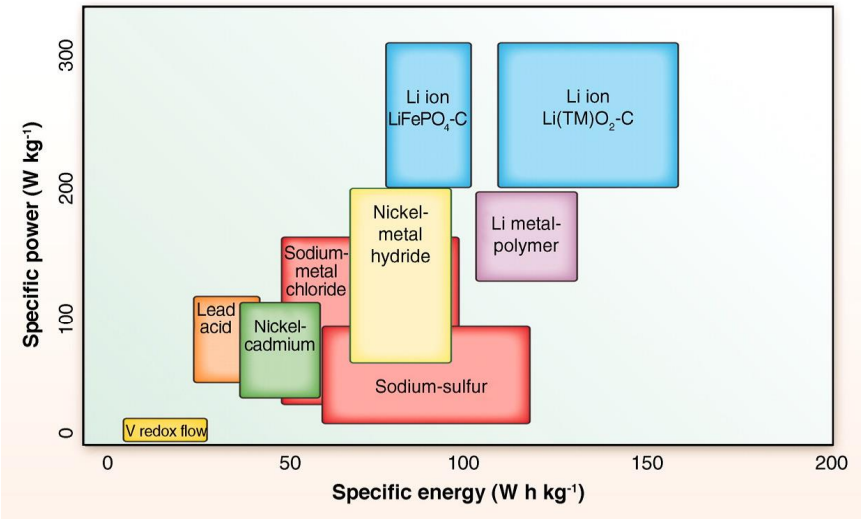

Figure 2.9: Power and energy densities of some battery technologies[57]

2.4.4 Li-based Battery

The history of Lithium-based battery technology goes way back to 1912, but it was not widely known until SONY made the commercial introduction of it in early 1990s[57]. They have developed it by using Li-intercalation compounds.
There are different types of Li-based batteries available. Classification among them is mainly based on the differences in their chemical composition. Among them, at least two types of devices are always clearly distinguished.

- **Lithium metal (liquid or polymer electrolyte)**: The anode, in this case, is composed of lithium (or an alloy of Li) and the cathode is made of an oxide (vanadium, manganese) or compounds based on chalcogen (sulfur). Batteries of this type have liquid electrolytes. Different problems were encountered after its introduction to market around the 1970s because of the behavior of the lithium electrode: passivation in contact with the electrolyte, formation of dendrites during cycling, etc. The life of cells currently available (small batteries) does not exceed a few hundred cycles at 10-20% DoD.

- **Lithium-ion (liquid or polymer electrolyte)**:The Li-ion battery system has a cathode (positive electrode), made of lithiated metal compound ($LiCoO_2$, $Li(NiCoAl)O_2$, $Li(NiMnCo)O_2$, $LiMn_2O_4$, $LiFePO_4$, etc.) and an anode (negative electrode), made of porous carbon (graphitic). These are isolated by a microporous separator made of polypropylene or polyethylene. During the charging process, a global transit of lithium-ion is established from the lithiated metal via the electrolyte ($LiPF_6$ salt dissolved in organic solvents) to the carbon matrix of the anode, where it accumulates. It undergoes oxidation during the discharge process, and a Li^+ circulation is established from the anode to cathode

in the accumulator, thus closing the circuit. Li-ion batteries have much longer cycle life than lithium metal batteries. In terms of energy and power density lithium-ion is also superior to lithium-metal batteries. So, discussion from this point will focus on Li-ion batteries only.

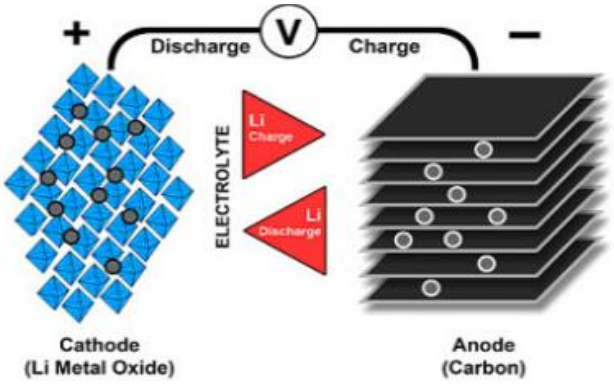

Figure 2.10: Ions shuttling in Li-ion battery[58]

Lithium has a low molecular weight, small ionic radius, and low redox potential[59]. Low redox potential allows the battery to provide high output voltage and high energy density. In fact, lithium-ion batteries outperform contemporary technologies by a factor of 2.5 in many extents. The technology has almost reached its maturity already, and many large projects (>1 MW) around the world have already been in operation to provide frequency support services. Some advantages and disadvantages of this technology are listed below[58]:

- **Advantages**
  - High specific energy and high loading capabilities
  - Less response time (in milliseconds)
  - Longer shelf-life, longer cycle life
  - Extremely low maintenance requirement
  - Low internal resistance, good coulombic efficiency
  - Higher energy efficiency
  - Simpler charging algorithm and shorter charging period
  - Very low self-discharge rate (maximum 5% per month)
- **Disadvantages or limitations**
  - Fragile and requires electronic management at each cell level to prevent thermal runaway as well as to ensure operational safety (limits the peak voltage while charging and stopping the cell voltage from becoming very low)
  - At high temperature, aging happens at a faster rate and lifetime gets shortened for deep discharge
  - Rapid charging is not possible at freezing temperature

- Maximum charging and discharging currents are limited to some extent
- Investment cost is significantly high

Having taken its limitations into account, it is obvious that precautions like cell temperature monitoring, limiting peak or trough voltages, etc. need to be adopted to reap the best benefits out of it.

Chapter 3

System Modeling

3.1 Proposed Microgrid

In this work, an all synchronous machine based system's performance will be compared with a less synchronous machine based, mostly power electronic converter dominated system. For that purpose, a microgrid has been proposed which resemble pretty much the grid usually found on an island. In the coming sections, the microgrid components and their modeling will be discussed in details.

3.2 Diesel Generator System

Generally, renewable source dominated systems lack inertia, damping, and reactive power capability. To address these issues in small grids like in microgrid, diesel generator system can be incorporated as a primary source of power supply. The main responsibility of diesel generator system is to maintain the frequency and voltage of the system within an acceptable limit. A diesel generator set mainly comprises an internal combustion engine(fueled by diesel), a governor, a synchronous generator and, an excitation system. The following figure gives an outline about the components of a diesel generator system. Here, V_t and I_t are terminal voltage and current and, E_f is the output voltage of the excitation block.

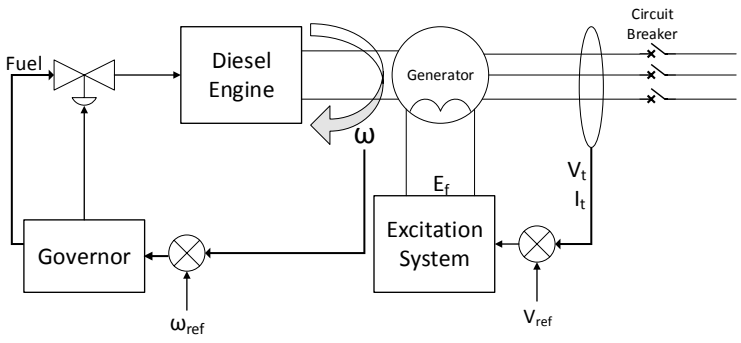

Figure 3.1: Schematic of Diesel-generator set

3.2.1 Diesel Engine

There are two main components in a diesel engine, one of them is a governor, and the other one is a reciprocating internal combustion engine.Diesel engine performs the duty of a prime mover. It drives the rotor through a coupling mechanism and thus provides mechanical input power to the synchronous generator coupled with it. The speed of the rotor shaft is controlled by a governor. Usually, there also exists a fuel actuator between the governor and the IC engine. Following diagram illustrates a little bit about diesel engine's important components. Here, F_L is fuel intake,ϕ is actuator's output and τ_m is the output torque.

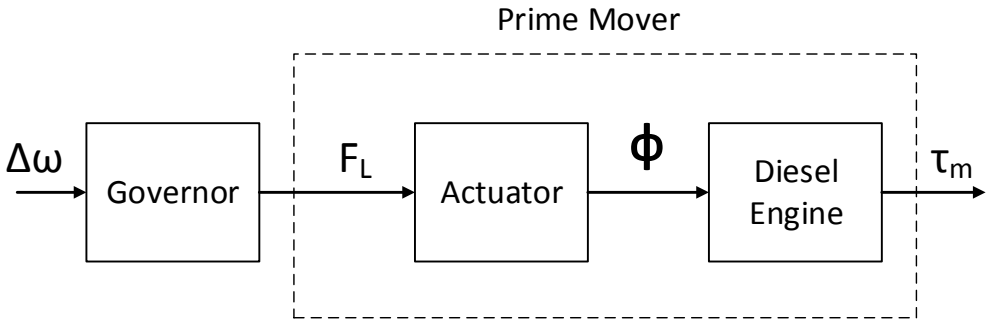

Figure 3.2: Schematic of Diesel Engine Components

There is a built-in IC engine model available in PSCAD library, which has been used to build the congregated model of a diesel generator set. It takes two inputs; the fuel intake F_L and shaft speed ω and outputs a mechanical torque τ_m which is fed to the synchronous generator. Here, the gear ratio has been selected as 1 which means that no gearbox is necessary, so the rotating speeds of the generator and engine are the same. The parameters of the diesel engine have been selected based on Cummins QSK78[62] diesel engine. Following table gives a brief overview of the parameters for the diesel engine.

Parameter	Value	Unit
Rated Speed	1800	rpm
No. of Cylinders	18	-
No. of Engine Cycles	4	Strokes
No. of Poles	4	-
No. of Misfired Cylinders	0	-
Engine Rating	2.0	MW
Machine Rating	2.5	MVA

Table 3.1: Diesel engine modeling parameters

Here, the machine rating is 25% bigger than the engine rating. It has been done so that the source can tackle sudden overload condition[60]. The amount of output mechanical torque, supposed to be fed to the generator's rotor shaft is dependent on a cylinder-torque angle curve[61]. The information of cylinder-torque

angle is already loaded in the IC engine model of PSCAD. Out of 36 available points on the torque angle plot, 24 points cylinder-torque angle plot has been selected for this work. The position of the cylinder or at which angle is it in depends on which stroke of a cycle is taking place. There are four of them namely, intake, compression, power and, exhaust. At the very beginning, the engine starts its cranking process where a signal from the system controller reaches to kick in the DC supply of the starter motor thus starting the intake stroke. The torque generated from the intake and exhaust strokes are pretty insignificant. Cranking process leads the engine to reach its firing speed where the combustion takes place. Before the combustion, the injected air gets compressed highly, and temperature goes up. At the time of compression, the torque is negative but soon after it reaches its highest value at power stroke. The torques generated by all the cylinders in the engine get summed up and give the aggregated diesel engine torque. To smooth out the ripples in the output torque, the number of cylinders has been increased to 18 in this case.

3.2.2 Governor

Governor is responsible for controlling the mechanical speed of the diesel engine. It performs this control task by regulating the fuel flow to the engine. This speed control mechanism implies that governor also has control over system frequency as that is proportional to the speed of the engine.

$$\omega_e = \frac{P}{2}\omega_m \tag{3.1}$$

Where,

ω_e [rad/s]= Electrical speed of the generator
P [-]= No. of poles of the generator

There are different types of governor mechanisms namely, a)'Isochronous' or constant speed governor, b)'Speed-droop' governor and, c) 'Speed-droop with power compensation' governor[63]. This classification has been made based on the difference in control mechanisms and type of feedback signals to compensate the speed deviation. In this work, the 'Speed-droop' governor has been used for speed compensation.
The 'Speed-droop' governor controls the mechanical torque input transmitted to the synchronous generator by controlling the gate position of the fuel valve through the fuel adjustment signal (F_L). The control block of the 'Speed-droop' governor is like the following in the figure below.

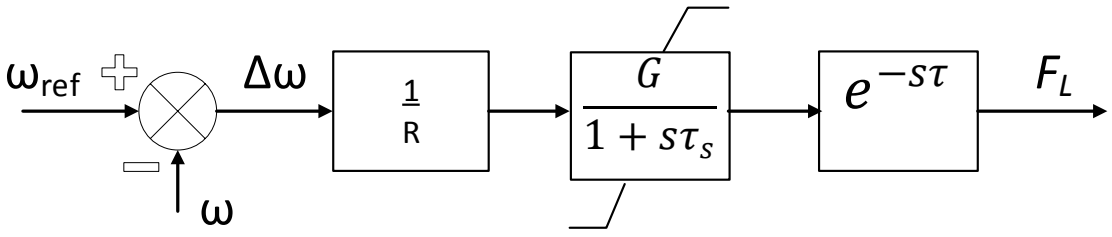

Figure 3.3: 'Speed-droop' governor control block

Here, R is the speed-droop coefficient, whose typical value ranges between 4%-5%. The control block represented by a transfer function is implementing an integral controller. It has a time constant τ_s, which characterizes the throttle actuator that controls the fuel flow. A limiter has been introduced to prevent the fuel flow from becoming negative or exceeding its maximum allowable limit. In addition to the control block, a time-delay or dead time (τ) has been used to delay the cylinder firing at the new throttle level at a particular speed. It has been done to ensure that every cylinder gets its fuel (as all of them are not in the same position to receive the fuel). The governor control block is pretty sensitive to load variations and frequency excursions and responds quickly to compensate the effect. Some values of the design parameters for the 'Speed-droop' governor are enlisted in the following table.

Parameter	Unit	Value
Speed-droop coefficient, R	-	5%
Dead-time,τ	s	0.02
Throttle actuation time, τ_s	s	0.1
Gain of the integral controller, G	-	1
Upper limit for the throttle actuation time	-	1
Lower limit for the throttle actuation time	-	0

Table 3.2: 'Speed-droop' governor design parameters

3.2.3 Excitation System

The excitation system of diesel generator comes with an exciter and an automatic voltage regulator. PSCAD has several built-in exciters in its library. All of these excitation systems' mathematical models have been given by IEEE which behave like commercial exciters. In this work IEEE AC1A excitation system has been chosen after comparing its performance with other available excitation systems. It is an alternator supplied rectifier excitation system and turns out to be more stable and takes less time to settle compared to its other counterparts. Here, the voltage regulator controls the switching of the rectifiers (thyristors). The exciter alternator is excited by itself. The rectifiers control the exciter's output voltage to produce direct current to be fed to the generator's field circuit. The system responds pretty fast. Rectifiers used in this system may be either stationary or rotating, depending upon the mode of power transmission to generator's field circuit. For example, if the field circuit gets energized via slip rings than stationary rectifiers are used, but for a brushless excitation system, rotating thyristors are utilized. A detail description of this system is given in[63]. The transfer function of this excitation system is shown in the following diagram. In addition to that, a description of some of the symbols and their values, provided by IEEE [64] are enlisted in the table below the picture.

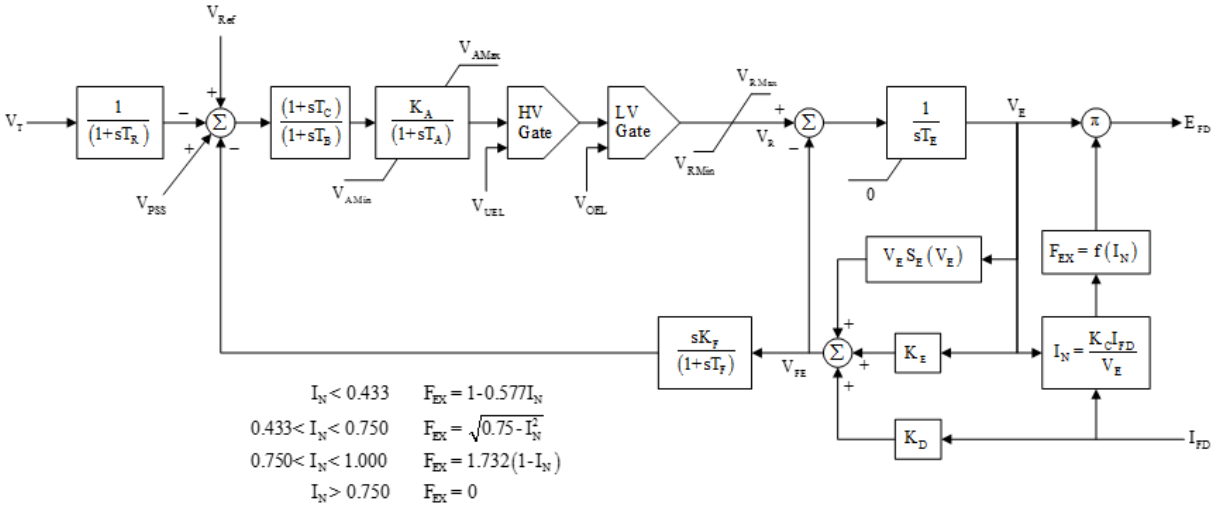

Figure 3.4: Transfer function of IEEE AC1A excitation system

Parameter	Value
Transducer time constant, T_R	0
Load compensating resistance, R_C	0
Load compensating reactance, X_C	0
Regulator gain, K_A	400
Regulator time constant, T_A	0.02
Lag time constant, T_B	0
Lead time constant, T_C	0
Maximum regulator internal voltage, V_{AMAX}	14.5
Minimum regulator internal voltage, V_{AMIN}	-14.5
Maximum regulator output voltage, V_{RMAX}	6.03
Minimum regulator output voltage, V_{RMIN}	-5.43

Table 3.3: IEEE AC1A excitation system parameters

3.2.4 Synchronous Generator

The synchronous generator is central to the diesel-generator system. A model of a nonsalient-pole synchronous generator has been chosen from PSCAD library and modified as per the requirement of test cases. This model is a detail electromagnetic transient representation of a synchronous generator and shows the electro-mechanical dynamics similar to the commercial one[65]. The model has been made based on park transformation in a stationary direct-quadrature (dqo) axis reference frame, which means that the design parameters have been projected to direct, quadrature and neutral axes. Eq. 2.2 has been adopted while modeling the generator along with a damping term. The damping is supposed to be provided by the quadrature axis damper windings of the generator, and that has been set to 2 here to quell the voltage spikes at

times of sudden load change. The no. of quadrature axis damper winding determines whether the machine will be salient pole or non-salient pole. After the incorporation of damping term, the swing equation of the generator turns out to be,

$$\tau_m - \tau_e = J\frac{d\omega}{dt} + D\Delta\omega \tag{3.2}$$

Here, D is the damping of the generator.

The inertia constant H has been set to 1.65 s as, [66] shows that diesel generators typically have an inertia constant ranging from 1.5 to 1.8 s. Some other design parameters of the synchronous generator are given in the following table.

Parameter	Unit	Value
Rated RMS line to neutral Voltage, V_{LN}	kV	7.9674
Rated RMS current, I_{Rated}	kA	0.104592
Base angular frequency, ω	rad/s	376.9911
Frequency droop constant, R	p.u.	0.05
Armature resistance, R_a	p.u.	0.002
Iron loss resistance	p.u.	300
D-axis synchronous reactance X_d	p.u.	1.79
D-axis transient reactance X'_d	p.u.	0.169
D-axis sub-transient reactance X''_d	p.u.	0.135
Q-axis synchronous reactance X_q	p.u.	1.71
Q-axis transient reactance X'_q	p.u.	0.228
Q-axis sub-transient reactance X''_q	p.u.	0.2

Table 3.4: Design parameters of the synchronous generator model

In this work, all the generators use local voltage and frequency measurement to adjust their production autonomously, following a system disturbance.

3.3 Load

The generic term load refers to a power consuming network component. It can be resistive, capacitive, inductive or a combination of any two or all of them. As per another classification criteria, loads can be i) constant power loads, ii) constant impedance loads and, iii) constant current loads. In this work, a constant power load rated at 6 MW has been used. In addition to that, the load has been assumed as a linear load. Typically, the power consumption by any load is closely related to system voltage and frequency, which is obvious from the equations below.

$$P = P_0\Big(\frac{V}{V_0}\Big)^{\mathrm{NP}} * (1 + K_{PF} * dF) \tag{3.3}$$

$$Q = Q_0\Big(\frac{V}{V_0}\Big)^{\mathrm{NQ}} * (1 + K_{QF} * dF) \tag{3.4}$$

Where,

P=Equivalent load real power

P_0= Rated real power per phase

V=Load voltage

V_0= Rated load voltage (RMS L-N)

NP=$\frac{dP}{dV}$=Voltage index for real power

K_{PF}=$\frac{dP}{dF}$=Frequency index for real power

Q=Equivalent load reactive power

Q_0= Rated reactive power per phase

NQ=$\frac{dQ}{dV}$=Voltage index for reactive power

K_{QF}=$\frac{dQ}{dF}$=Frequency index for reactive power

For implementing a constant power load model, parameters NP, NQ,K_{PF} and, K_{QF} have been set equal to zero. Constant power loads vary their impedances in response to the change of input and maintain its power consumption constant. So, to model that, variable resistors and inductors are used[67].

3.4 Distribution Lines

As the size of the grid under consideration is pretty small, a short transmission line has been used to represent the medium for carrying power among the components of the power network. Usually, a PI model of the transmission line is used in most of the cases, but PI models only comprise passive elements and don't represent propagation delay. There are three types of modeling schemes available in PSCAD and as per their suggestion, 'Frequency dependent (Phase)' mode is the best one[68]. In this work 'Frequency dependent (Phase)' distributed model has been used to represent all of the frequency dependent effects of the transmission line. Following table contains a short description of the design parameters and their values for the transmission line used in this case.

Parameter	Unit	Value
Length of the line	km	5
Steady state frequency	Hz	60
Number of conductors	nos.	3
Height of lowest conductors	m	13
Horizontal spacing between conductors	m	1.5
Vertical offset of the center conductor	m	0.5
Sag	m	1.5
DC resistance	Ω/km	0.3712
Outer radius	mm	10

Table 3.5: Distribution line design parameters

3.5 PV System

The role of PV system, in this case, is to produce constant power throughout the simulation time-frame. To arrange that a very simple technique has been used to represent the PV system model. A controlled current source has been used to represent both the PV modules and DC-DC converter system. The reference current (I_{ref}) for the dependent current source is obtained from an algorithm which incorporates the reference real power level and reference set point for DC link capacitor's voltage (V_{DC}). There exists a regulation mechanism for the DC link voltage as well. A voltage sourced converter (VSC) has been used to interface the controlled current source to the rest of the grid. The design of the VSC and the L-C-L filter inside it will be discussed in the coming section.

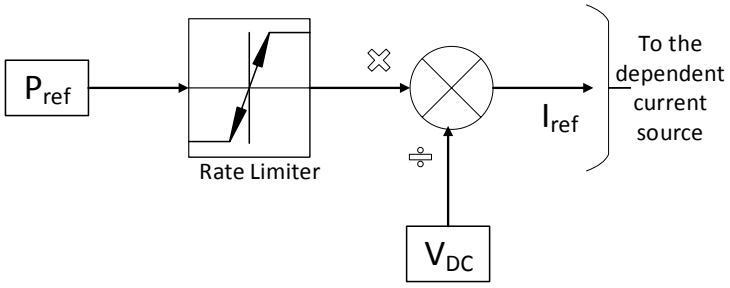

Figure 3.5: Reference current generation for the PV system

3.6 Phase Locked Loop (PLL)

One of the most important components in the proposed microgrid is phase locked loop or PLL. It is a non-linear measuring device and measures voltage phase displacement and system frequency. These information are very important as they are supposed to be used to control grid side converters and to synchronize power electronic converter based energy sources to the grid. There are three types of PLL available to measure the phase. They are i) zero-crossing, ii) stationary reference frame and, iii) synchronous rotating reference frame (SRF). Among the three, the SRF works best at distorted and non-ideal grid conditions[69] and, that's why SRF PLL has been selected for this work.

The basic structure of a PLL contains some transformation blocks, a loop filter and a voltage controlled oscillator (VCO). The detected phase angle is used for computation by the transformation blocks via a feedback control system that tracks the phase angle. The difference between the measured signal and desired one is compensated through a PI controller which performs as a low pass loop filter as well. There exists a voltage controlled oscillator which yields the phase. Overall, the system voltages are fed as inputs to the PLL system, and it outputs the phase angle. The concept of PLL has been illustrated a little more in the following figure.

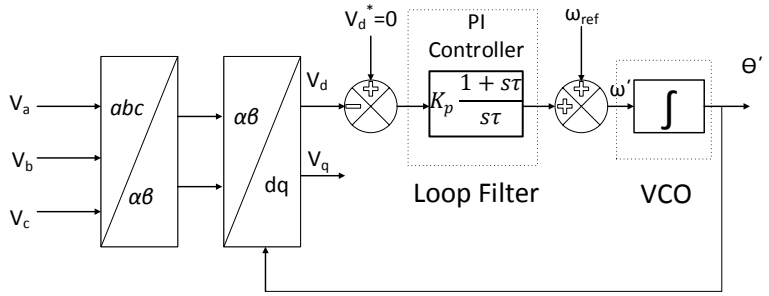

Figure 3.6: Structure of the SRF-PLL System

Here, each phase of the three-phase voltage signal has been converted to a stationary system of two phases V_α and V_β. This transformation is known as 'Clark transformation'.

$$V_{\alpha\beta} = T_{\alpha\beta} V_{abc} \tag{3.5}$$

Where, $T_{\alpha\beta}$ is a matrix operator.

$$T_{\alpha\beta} = \frac{2}{3}\begin{bmatrix} 1 & \frac{-1}{2} & \frac{-1}{2} \\ 0 & \frac{-\sqrt{3}}{2} & \frac{\sqrt{3}}{2} \end{bmatrix}$$

So, the operation turns out to be,

$$V_{\alpha\beta} = \begin{bmatrix} V_\alpha \\ V_\beta \end{bmatrix} = T_{\alpha\beta} \begin{bmatrix} V_m sin(\theta) \\ V_m sin(\theta - \frac{2\pi}{3}) \\ V_m sin(\theta + \frac{2\pi}{3}) \end{bmatrix} = \begin{bmatrix} V_m sin(\theta) \\ V_m cos(\theta) \end{bmatrix} \tag{3.6}$$

These V_α and V_β are again transformed to direct and quadrature axis through park transformation.

$$\begin{bmatrix} V_q \\ V_d \end{bmatrix} = T_{qd} \begin{bmatrix} V_\alpha \\ V_\beta \end{bmatrix} \tag{3.7}$$

Where,

$$T_{qd} = \begin{bmatrix} sin(\theta^{'}) & cos(\theta^{'}) \\ -cos(\theta^{'}) & sin(\theta^{'}) \end{bmatrix}$$

Here, $\theta^{'}$ is the estimated phase angle output of the PLL block. After going through the park transformation, the direct and quadrature axis voltage components take the following form.

$$\begin{bmatrix} V_q \\ V_d \end{bmatrix} = \begin{bmatrix} V_m cos(\theta - \theta^{'}) \\ -V_m sin(\theta - \theta^{'}) \end{bmatrix} \tag{3.8}$$

The PI controller (shown in figure 3.6) has a gain which makes V_d following the reference set-point $V_d^* = 0$. If V_d becomes zero then the synchronization becomes complete and estimated frequency $\omega^{'}$ is locked with

the system frequency ω. Similarly, estimated phase angle $\theta^{'}$ follows system phase angle θ. Following table shows the values of some of the parameters used to design the PLL.

Parameter	Value
Base Frequency	60 Hz
Proportional Gain	50
Integral Gain	900

Table 3.6: Phase locked loop (PLL) design parameters

In this work, PLL has been used to track system frequency which is then used to control the charging current of BESS. It also plays a vital role in the control system of VSCs.

3.7 DC Link Capacitor

To ensure constant power exchange in both direction (from the grid and to the grid) some intermediary energy storage device is required. DC link capacitor fulfills the need of the energy storage device. To ensure almost constant power exchange, the voltage across the DC-link capacitor is always kept constant irrespective of the magnitude and direction of the exchange. The direct axis component of the input current from the grid is responsible for maintaining the constant voltage across it. Picking up the perfect sized capacitor is a key factor and is very important from the perspective of whole system design.
While designing any capacitor, the equation which forms the basis of the design criterion is as follows.

$$i_{cap} = C\frac{dV_{dc}}{dt} \tag{3.9}$$

Where,

i_{cap}=Current going through the capacitor

C= Capacitance of the capacitor

dV_{dc}= Derivative of the voltage across the capacitor, V_{dc}

Therefore, the expression to find the capacitance of the dc-link capacitor becomes,

$$C = \frac{i_{cap}dt}{dV_{dc}} \tag{3.10}$$

The denominator dV_{dc} is the voltage ripple or oscillating voltage amplitude, often chosen as 10% or 20% of the maximum value of the nominal dc link voltage. The calculations that govern the designing of dc-link capacitor are:

- Calculation of capacitance for a given tolerable voltage ripple
- Calculation of the rms current ripple through the capacitor for the worst case

There are several topologies available to calculate the dc-link capacitance value, and they are mainly dependent on which type of topology is used to control the corresponding converter/inverter. As here in this work

the SPWM topology has been used for the inverters, so necessary scheme described by [70] has been used to accomplish the design of dc-link capacitor. It is pretty obvious from the above equation that the lower the capacitance, the higher the voltage ripple will be. But higher voltage ripple will introduce more harmonics into the system and, on the other hand, the bigger capacitor is expensive. So, a trade-off is required between the two.

A proper expression for the numerator of the above equation is also required to find the capacitance. That can be achieved by integrating either the positive or negative part of i_{cap} in one switching period. This is done so, as integrating over a whole switching cycle will not help too much as the result will come out as zero as the capacitor doesn't have a DC current offset. The current through the capacitor can be calculated with the help of the following formula given by [71] .

$$i_{cap} = \sqrt{\frac{3I_N^2 M}{4\pi}(\sqrt{3} + cos(2\phi)(\frac{2}{\sqrt{3}})) - \frac{9}{16}(I_N M)^2 cos^2(\phi)} \tag{3.11}$$

Where,

M=Modulation index

I_N= Amplitude of the output or input current of the converter/inverter

ϕ=Power factor angle

Here, the target is to operate the system at unity power factor ($\phi = 0$), so modulation index M has to be chosen in such a way so that, the capacitor can sustain the worst possible condition in terms of forbearance the maximum current through it. According to [70], M=0.667 at p.f =1 gives the maximum value of the numerator in equation 3.10, so in this work, 0.667 has been chosen as the value for M. The ripple voltage dV_{dc} can be expressed in terms of dc voltage ripple requirement (ϵ).

$$dV_{dc} = \epsilon V_{dc} \tag{3.12}$$

And, dt is set equal to half of the switching period based on the above argument. So, eventually, the expression to find dc-link capacitance evolves from equation 3.10 to the following form.

$$C = \frac{i_{cap} T_{sw}}{2\epsilon V_{dc}} = \frac{i_{cap}}{2\epsilon V_{dc} f_{sw}} \tag{3.13}$$

Here, T_{sw} is the switching period of the converter or inverter and f_{sw} is the switching frequency. The energy exchanged with the dc-link capacitor is much greater than the energy exchanged with the coupling inductor. So, while designing the dc-link capacitor, the inductor hasn't been taken into account. Sometimes, an extra resistor is added in series to the dc-bus along with an IGBT to dissipate excess energy that is generated during a grid fault. This arrangement is termed as 'dc-crowbar' or 'dc-link chopper,' but this is also kept beyond the scope of this work.

3.8 L-C-L Grid Side Filter

An L-C-L filter is used to interface the voltage source converter (VSC) to the grid or rest of the system. Its main function is to suppress the harmonics produced from the switching of the converter or inverter.

Harmonics are harmful as they create disturbances to sensitive devices and produce extra losses. There are L filter , LC filter, etc. topologies to eliminate harmonics introduced from switching but LCL filter has better attenuation capability to suppress higher order harmonics, and it can lower current ripples flowing through the grid-side inductor.

To find out the filter parameters, the base impedance needs to be figured out which will help to find the capacitor's capacitance of the filter. If V_n is the line to line RMS voltage of the inverter (grid side) and S_n is the MVA rating of the inverter then, base impedance becomes[72, 73]:

$$Z_b = \frac{V_n^2}{S_n} \tag{3.14}$$

Base capacitance C_b can then be described in terms of base impedance, Z_b.

$$C_b = \frac{1}{\omega_n Z_b} \tag{3.15}$$

Here, ω_n is the nominal grid angular frequency. To determine the exact size of the filter capacitor (C_f), the maximum allowable power factor variation is considered. It is a trade-off between the main inductor's (inverter side) current handling capability and the required reactive power. Usually the filter capacitor is set equal to 5-6% of the base capacitance[74].

$$C_f = 0.05 C_b \tag{3.16}$$

The main inductor's (inverter side) inductance is dependent on output ripple current (ΔI_{L-max}),dc-link voltage (V_{dc}) and switching frequency (f_{sw}) and can be expressed in terms of them like the following[75]:

$$L_i = \frac{V_{dc}}{8 \Delta I_{L-max}} \tag{3.17}$$

The value of ripple current has been set equal to 20% which is considered as a good trade-off between inductor size and ripple current amount[76]. So, the expression of current ripple is specified as,

$$\Delta I_{L-max} = 0.02 \frac{P_{rated}\sqrt{2}}{\sqrt{3} V_n} \tag{3.18}$$

Here, P_{rated}, is the rated active power of the inverter. The grid side inductance (L_g) should have an inductance which can put some control on the voltage drop across it. For finding a proper value for it, a relation between inverter side and grid side inverter can be used as per [74], which says to use $\frac{L_i}{L_g} = 3$.

While designing the filter, finding its cut-off or resonance frequency is very much important. The resonance frequency of the filter should stay in a range between ten times the grid frequency and one half of the switching frequency of the converter or inverter. It is chosen like this so that the filter doesn't get excitation by the converter voltage harmonics[73]. There is another reason for choosing the resonance frequency like that, which is, the filter should have enough attenuation in the range of the switching frequency. The

resonance frequency of the filter is given by,

$$f_{res} = \frac{1}{2\pi}\sqrt{\frac{L_i + L_g}{L_i L_g C_f}} \tag{3.19}$$

The LCL filter magnifies frequencies around the resonant frequency. To suppress those, a damping resistor can be used which may not be the best solution always as it increases the heat loss and decreases the efficiency of the filter system. Here, in this case, the damping resistor has not been included.

3.9 Voltage Source Converter (VSC)

The voltage source converter is one of the most important components of the power conversion system. It accomplishes the power transfer between grid and BESS. In this work, the VSC has been placed in between the grid and DC-DC converter. It is responsible for keeping the voltage across the dc-link capacitor constant. The VSC under discussion is a three-legged converter. It has six high-frequency switches (IGBT) that perform the DC to AC or AC to DC conversion. Each IGBT has an anti-parallel diode connected with it. These IGBTs are controlled via some gate pulses generated by the controller which is the central part of VSC. For this case, a sinusoidal pulse width modulation (SPWM) technique has been chosen. A vector current control approach has been adopted to generate the reference signals for producing the switching signals.
The VSC control strategy is based on an inner current control loop. The scheme utilizes a two-axis synchronous reference frame (dq). The ac current vector of VSC is decomposed into direct (I_{d}) and quadrature axis components (I_{q}) by park transformation.

$$\begin{bmatrix} I_d \\ I_q \\ I_o \end{bmatrix} = \frac{2}{3}\begin{bmatrix} cos(\theta) & cos(\theta - \frac{2\pi}{3}) & cos(\theta + \frac{2\pi}{3}) \\ sin(\theta) & sin(\theta - \frac{2\pi}{3}) & sin(\theta + \frac{2\pi}{3}) \\ \frac{1}{2} & \frac{1}{2} & \frac{1}{2} \end{bmatrix}\begin{bmatrix} I_a \\ I_b \\ I_c \end{bmatrix} \tag{3.20}$$

The real or direct axis component regulates the capacitor voltage, and quadrature axis component is responsible for keeping the terminal voltage on the grid side at a constant level. The benefit of using synchronous rotating reference frame is that the projected parameters are all DC, in a balanced sinusoidal steady state. The phase angle of ac phase voltage has been used as the reference phase angle to conduct the transformation. A PLL has been used to extract the reference phase angle information. The greatest advantage of using PLL is that it can ceaselessly synchronize the output frequency and phase voltage of the grid with grid current. So, output and input phases are always matched up.
The current components are fed into regulators which produce the reference set point for direct (${V_{\mathrm{d}}}^*$) and quadrature axis (${V_{\mathrm{q}}}^*$) voltage components. In fact, the measured dc-link voltage is compared with a reference dc-link voltage. The error is then compensated by a PI controller which produces reference direct axis current component(I_{dref}). Quadrature axis reference current (I_{qref} is calculated in a similar fashion but from reactive power information. Reference signals for modulation are created by performing inverse park transformation on ${V_{\mathrm{d}}}^*$ and ${V_{\mathrm{q}}}^*$ along with some post-processing. The modulating waves are compared with a 2.5 kHz triangular carrier signal with magnitude ranging between +1 and -1. Switching signals GG1, GG3 and, GG5 are produced via a comparator. The comparator produces an output 1 when the reference modulating signal is greater than the carrier signal and produces 0 for other conditions. Operation of the

two switches on each leg of the VSC is complementary to each other. That's why the switching signals GG2, GG4 and, GG6 are produced by inverting GG1, GG3 and, GG5 respectively. Following diagram illustrates the VSC structure to some extent.

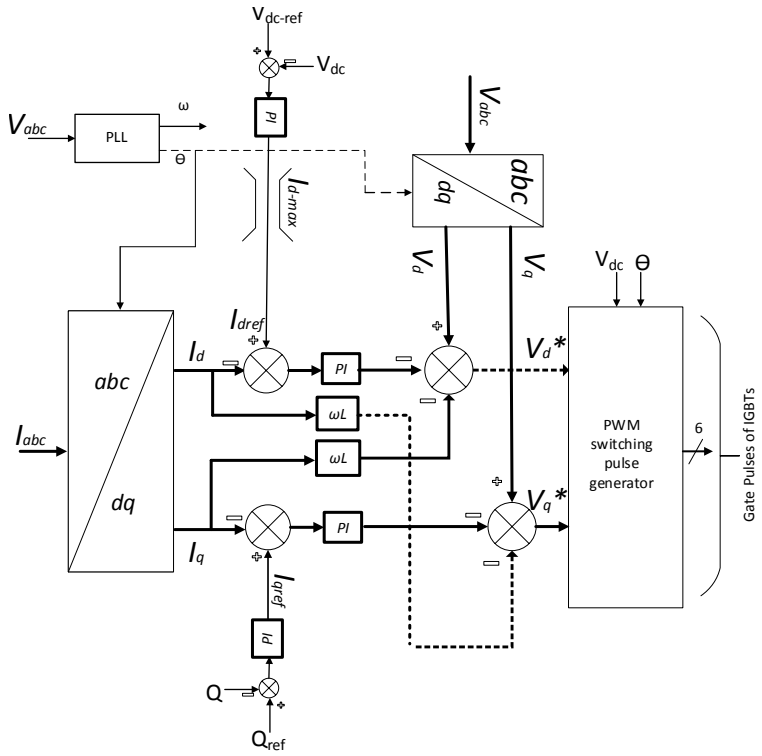

Figure 3.7: VSC control algorithm

The active (P) and reactive (Q) power flow through the VSC are related with the direct and quadrature axis components and can be expressed like the following.

$$P = \frac{3}{2}(V_d I_d + V_q I_q) \tag{3.21}$$

$$Q = \frac{3}{2}(V_q I_d - V_d I_q) \tag{3.22}$$

The grid voltage is aligned with the direct axis of the synchronous reference frame which implies that the quadrature axis component is equal to zero ($V_q = 0$). That makes the above expression of real and reactive power look like the following.

$$P = \frac{3}{2}V_d I_d \tag{3.23}$$

$$Q = -\frac{3}{2}V_d I_q \tag{3.24}$$

So, it is pretty obvious from the above expression that real and reactive power transfer will be proportional to direct axis and quadrature axis currents as the grid voltage remains almost constant all the time.

3.10 Buck-boost Converter

To achieve better controllability on power exchange, two-level converter topology has been adopted in this work. Buck-boost converter provides the control to power exchange at the dc-side and can provide bi-directional power transfer capability. During charging of the BESS the converter operates at buck mode and at discharging stage, it operates at boost mode. Whether the battery will operate in charging mode or discharging mode, is set manually in this work but, that also can be replaced by some automatic control topology. This work mainly focuses on the charging stage of the BESS. For that reason, only buck mode operation will be discussed in this section.

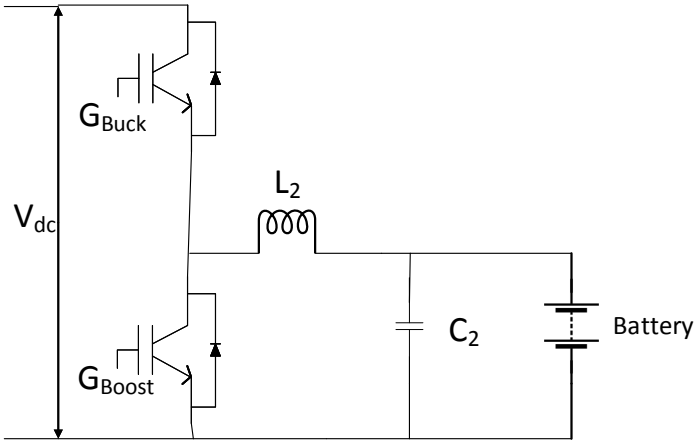

Figure 3.8: Bi-directional DC-DC converter

Irrespective of charging and discharging mode, the voltage across the dc-link capacitor is almost always constant. So, during the duration of charging, the voltage across the batteries are lower than the dc-link voltage (buck mode). Usually, the duty cycle (D) tells about the ratio of these two voltages, but depending on the control mechanism this relation may change.

$$\frac{V_{BESS}}{V_{dc}} = D \tag{3.25}$$

A small L-C filter exists between the converter and the BESS. It eliminates the harmonics created by the switching of the converter. The inductor current of the filter is regulated by the control mechanism of the buck converter so that it can not exceed the maximum charging current of the battery. To design the L-C filter parameters, the limit on battery charging current and allowable voltage ripple have been taken into consideration. For inductor, it must be designed in such a way that it can withstand the maximum possible charging current for the battery pack which will come from the battery capacity (A-h rating) and it's nominal voltage ($V_{battery}$). Assuming charging happens both in continuous and discontinuous conduction modes, the inductor size can be achieved from the following relation suggested by[77]:

$$L\frac{dI}{dt} = V_{battery} \tag{3.26}$$

$$L\frac{2\Delta I_L f_{sw}}{D} = V_{battery} \tag{3.27}$$

Here, ΔI_L is the inductor current ripple. Switching frequency is chosen to be 2.5 kHz. While determining the size of the capacitor, it has been assumed that 10% ripple will be allowed in voltage at full loading condition.

$$C\frac{dV}{dt} = I_{Load} \tag{3.28}$$

$$C\frac{0.1V_{dc} f_{sw}}{D} = I_{Load} \tag{3.29}$$

There is an alternative approach to find the value of the inductance and capacitance of the L-C filter at the battery end proposed by[78].

$$LC = \frac{(V_{dc} - V_{battery})V_{battery}}{8{f_{sw}}^2 V_{dc}\Delta V_{battery}} \tag{3.30}$$

One of them, either inductance or capacitance is chosen as per the commercially available rating, then the other one can be easily found from the above relation and the product on the right-hand side of the equation.

3.10.1 Proposed Battery Charge Controller

The provision of inertial and droop response is accomplished with the help of the charge controller of the battery pack. This is done by modifying the gate pulses to the buck converter according to some control approach. Usually, there exist several charging strategies to charge the battery namely, constant-current charging (CC), constant-voltage charging (CV), constant current followed by constant voltage charging topology, etc. Here, in this case, constant current charging has been adopted to implement the proposed algorithm. The reason for choosing that one is that while charging the battery voltage doesn't change much and remains almost constant.

Following a disturbance in the system, the system frequency undergoes a downward event. The amount of deviation of the frequency from its nominal value is related to the active power mismatch between generation and load. The battery, in this case, is considered as a smart load which can respond to resolve the frequency excursion. It responds according to some algorithms which make it provide ancillary services; inertial response and droop response. In fact, in the proposed control algorithm, the following equation has been implemented.

$$P_{BESS} = K_p(f_{ref} - f) + K_d\frac{df}{dt} \tag{3.31}$$

To implement equation 2.15, the system frequency is measured via a PLL. The received signal is usually noisy, so a low-pass filter is used to smooth out the frequency signal. Then two operations are conducted on this received signal; it is compared with the nominal system frequency, and it's derivative is taken. The result from the comparison is fed to the droop control algorithm section where the frequency error is multiplied with a droop coefficient K_p. The value of droop coefficient is calculated from the real power rating of the battery pack and the amount of droop expected from it. It is a negative quantity and denotes that it is

counteracting the frequency deviation.

The frequency derivative term is used to emulate inertial response; it is multiplied with an inertial coefficient K_d, whose value is determined from the expected inertia emulation level and system base. This is also a negative quantity denoting that it counteracts the rate of change in system frequency. Both products of the multiplication represent active power to be shed from the battery's real power consumption. Before the fault event takes place, the battery is supposed to charge at a pre-defined constant current. The total power to be shed is divided by the battery terminal voltage; the process yields an amount of current. This amount is subtracted from the pre-defined set-point of the charging current. Following figure illustrates the charging control topology in detail.

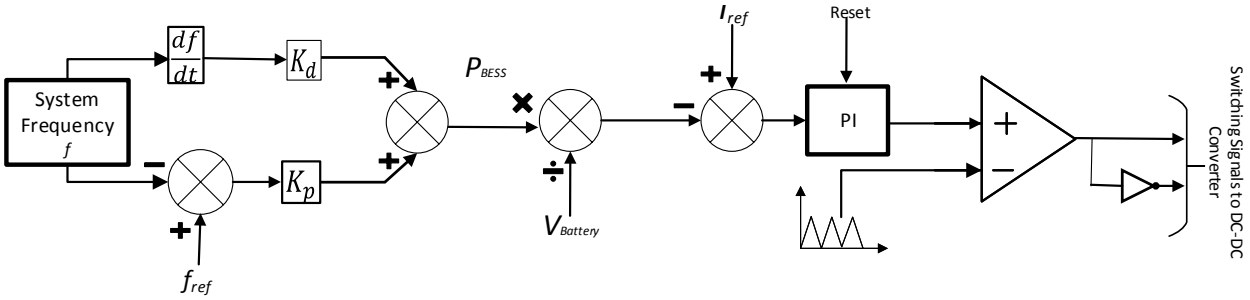

Figure 3.9: Charging current controller of BESS.

There exists an over-current protection system that protects the buck converter and the battery pack from high currents. The limit for highest allowable charging current is set to a certain value to implement this scheme. A reset command is generated if the charging current exceeds the maximum allowed value. The schematic representation of the algorithm is given in the following figure.

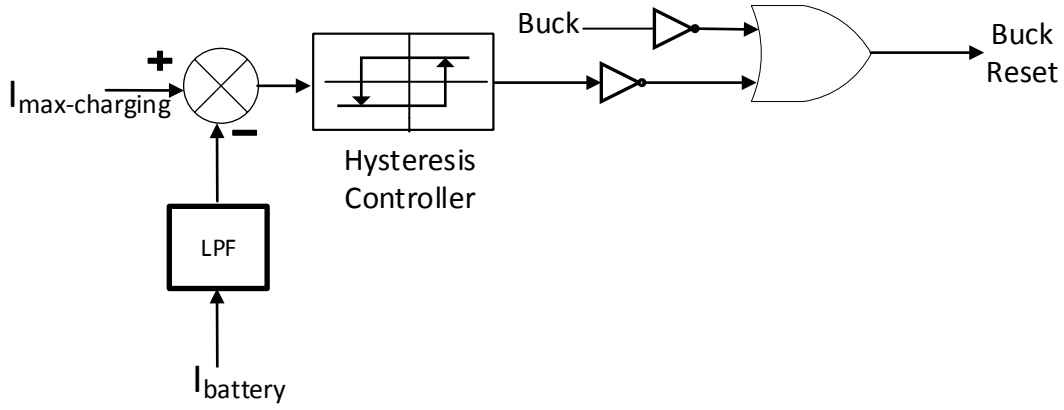

Figure 3.10: Overcurrent protection scheme

The design parameters for the modified battery charge controller is given in the following table.

Parameter	*Symbol*	*Value*	*Unit*
Droop Coefficient	K_{p}	1333	kWs
Inertia Coefficient	K_{d}	275	kWs^2
Switching frequency, buck converter	f_{sw}	2.5	kHz
Proportional gain, buck converter	K_{pBuck}	100	-
Integral gain, buck converter	K_{iBuck}	1000	-

Table 3.7: Charging Current Controller Parameters

3.11 Battery Energy Storage System

The battery model used in this case has been taken from PSCAD library. It's a Lithium-ion battery model which has been developed based on the equation given by 'Shepherd'[79] with some modification[80]. It is an electric circuit based model and represents the electro-chemical behavior of the battery pretty well. The model proposed by 'Shepherd' has incorporated battery terminal voltage, open circuit voltage (OCV), internal resistance, discharge current and state of the charge (SOC) of the battery but here, only SOC of the battery has been used as the state variable.
What is central in the battery model, is a controlled voltage source connected in series with a constant internal resistance (R_{bat}). The open circuit voltage of the battery is calculated from a non-linear equation.

$$E = E_0 - K(\frac{Q}{Q - it}) + Ae^{-Bit} \tag{3.32}$$

Where,

$E[V]$=No-load voltage
$E_0[V]$= Constant voltage of the battery
$K[V]$=Polarization voltage
$Q[A-h]$= Battery Capacity
$it[A-h]$=Actual battery charge
$A[V]$=Exponential zone amplitude
$B[(A-h)^{-1}]$=Exponential zone time constant inverse

A figure representing the equivalent electrical circuit of the battery is given below. The aforementioned equation has been implemented as a part of the control approach of the battery's internal circuit.

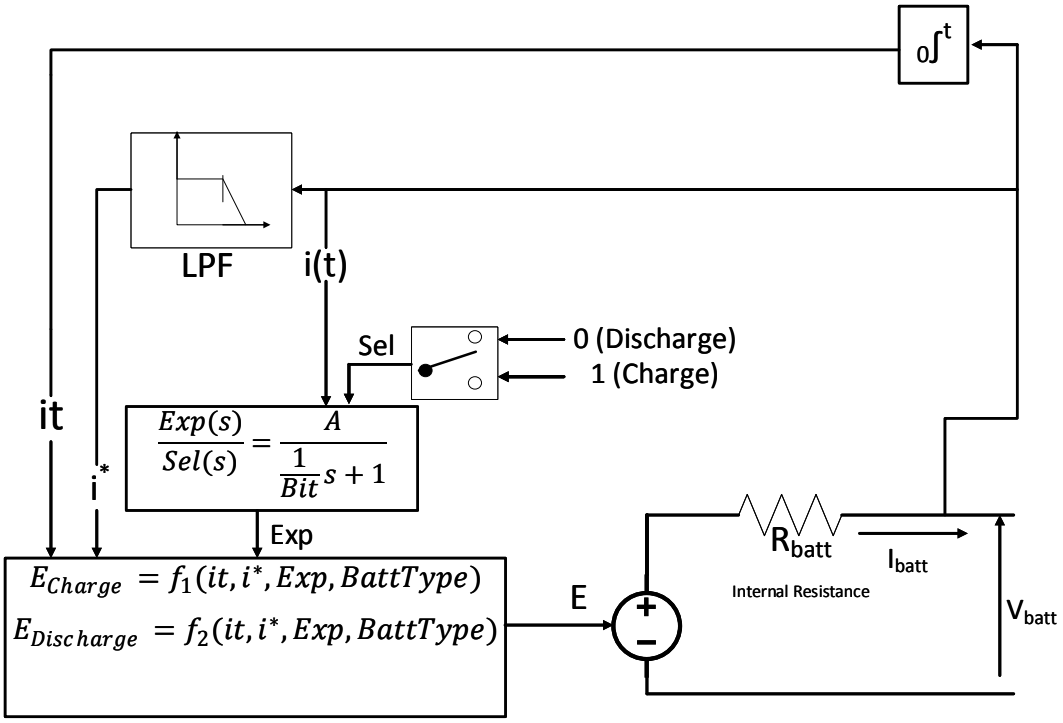

Figure 3.11: Equivalent Circuit of the Battery

To properly understand the parameters A and B, a closer look at battery charge or discharge characteristics is necessary. Following figure represents a typical discharge curve of a Li-ion battery where the exponential zone is highlighted in green color.

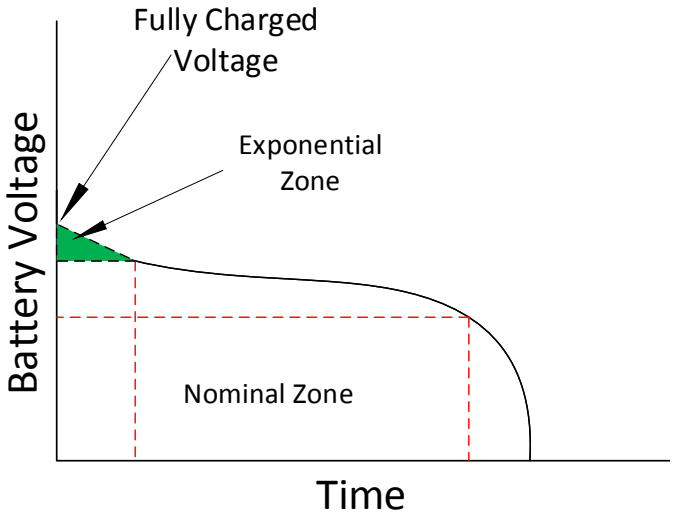

Figure 3.12: Discharge Characteristics of the Battery

Both the charge and discharge cycles for the battery are assumed to have same characteristics in this model under use so, curve showing charging characteristics will also look like the same except with a horizontal flip. As it has been mentioned earlier that the battery model only takes SOC as the state variable so the above equation can be modified like the following:

$$E = E_0 - K(\frac{1}{SOC}) + Ae^{-BQ(1-SOC)} \tag{3.33}$$

So, the SOC will contribute to the battery voltage both in exponential term and in non-linear term implying that the battery voltage is entirely dependent on SOC of the battery.
The battery model under discussion has been developed through some assumptions, and it has some shortcomings as well[80]. They are listed in the following.

Assumptions

- Internal resistance of the battery is assumed constant both in charging and discharging stage. The amplitude of battery current doesn't affect it.
- Design parameters are assumed to be the same both in charging and discharging stage.
- Charging and discharging doesn't have any effect on battery characteristics (No memory effect , No hysteresis).
- Self-discharge of the battery has not been taken into account.
- Temperature doesn't have any effect on the model's behavior.
- Peukert effect has been ignored.

Limitations

- Battery voltage cannot become negative, and there is no upper bound for battery voltage.
- The minimum capacity of the battery is 0 A-h, and there is no upper limit of the battery capacity though, charging stops when SOC reaches 100% in this case due to the charge control algorithm.

3.11.1 Extraction of the Design Parameters for the Battery

Various parameters of the battery model have been found as per the suggested approach of [80].

Internal Resistance

To measure the voltage drop in the equivalent electrical circuit for varying current, it is very important to know the rating of battery's internal resistance. It affects the output voltage and efficiency (η) of the battery. When no other information is available , the internal resistance of the battery (R_{batt}) can be determined by the following relation:

$$R_{batt} = V_{rated}\frac{1-\eta}{0.2Q_{rated}} \tag{3.34}$$

Here, V_{rated} is the rated voltage of the battery and Q_{rated} is the rated capacity of the battery in A-h.

Three Points on the Characteristics Curve of the Battery

The exponential part Ae^{-Bit} can be calculated if the two points A and B of the characteristics curve can be found. Among them point A (voltage drop in the exponential zone) can be found from the following relation,

$$A = E_{Full} - E_{Exp} \tag{3.35}$$

Here, E_{Full}, is the amplitude of the fully charged voltage and E_{Exp} is the end of the exponential zone voltage. The other parameter of the battery voltage equation B can be got from the following relation.

$$B = \frac{3}{Q_{Exp}} \tag{3.36}$$

Q_{Exp} is the charge at the end of the exponential zone.
The polarization voltage, K is determined from the non-linear battery voltage equation.

$$K = \frac{(E_{Full} - E_{rated} + A(e^{-BQ_{rated}} - 1))(Q - Q_{rated})}{Q_{rated}} \tag{3.37}$$

The battery constant voltage is calculated from the expression below.

$$E_0 = E_{Full} + K + iR_{batt} - A \tag{3.38}$$

Chapter 4

Study Cases and Simulation Results

4.1 Overview

To explore whether the BESS can emulate synchronous generator's behavior to compensate for frequency excursions or not, several study cases will be examined in this chapter. As the goal is to compare with the conventional power system, two types of customized microgrid will be checked. One, with only synchronous diesel generators with no inverter-based power source, another one with less number of synchronous generators, PV plant, and BESS. Unlike other literature in this area, the penetration of distributed energy resource is much higher in this case (almost 60%). So, it will be worth taking a look whether the customized microgrid can operate satisfactorily or not, with having the control algorithm incorporated.
All the customized microgrids along with their components are modeled and simulated in PSCAD (version 4.6.2). All of the simulations have been run for 25 seconds with a solution time step of 5 μ-second. The time step has been chosen as 5 μ-second to maintain similarity with real-time simulators like RTDS, which usually adopts solution time steps ranging around 1-4 μ-second for simulation of fast-switching power electronic devices[81]. While in simulation, a generator has been tripped after 10 seconds of the simulation for both types of microgrid. The loss of generation results in a loss in equilibrium between demand and generation and the effect is visible on the system frequency. The main two parameters in focus are, the amount of frequency deviation and the rate of change in frequency (ROCOF). To judge and compare the system performance for providing inertial and droop response, four study cases have been performed.

- **Study Case I:** Studies the system's response towards a loss of generation event. Here, the microgrid under use is an all synchronous generator based system.
- **Study Case II:** Examines the system's performance to compensate for frequency deviation with less conventional generators. There exist several inverter based power generating units and load. Only droop control algorithm has been activated.
- **Study Case III:** Uses same system components like case II but with both inertial and droop control algorithm activated.
- **Study Case IV:** Both inertial and droop control algorithm activated but with a modification in inertial response algorithm. The rising part of ROCOF has been excluded from the feedback response.

4.2 Study Cases

4.2.1 Study Case I

In this study case, a microgrid has been constructed with only conventional generators.Four diesel generators have been used to serve that purpose. Each one is rated at 2.0 MW and is operating at 1.5 MW. The machine rating is chosen to be 2.5 MVA. A linear load rated at 6 MW is fed by the four generators. Each generator is sharing the load equally as they all have the same rating or size. Following figure gives a layout of the model for study case I.

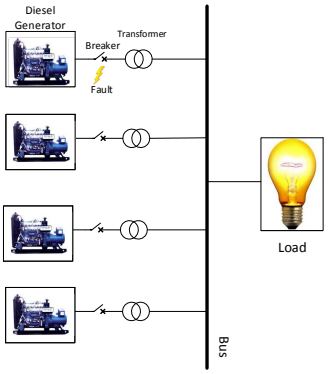

Figure 4.1: Layout of the model for study case I

After 10 seconds a generator is tripped from the system, as a result of that, 2 MW generation is lost. The remaining three generators increase their output from around 1.5 MW to 2 MW, to serve the load. The increased demand is shared equally by all three of them as they are of the same size and are supposed to provide same 5% droop . The figure given below shows how each one of the remaining generators increases their power generation in response to the system disturbance.

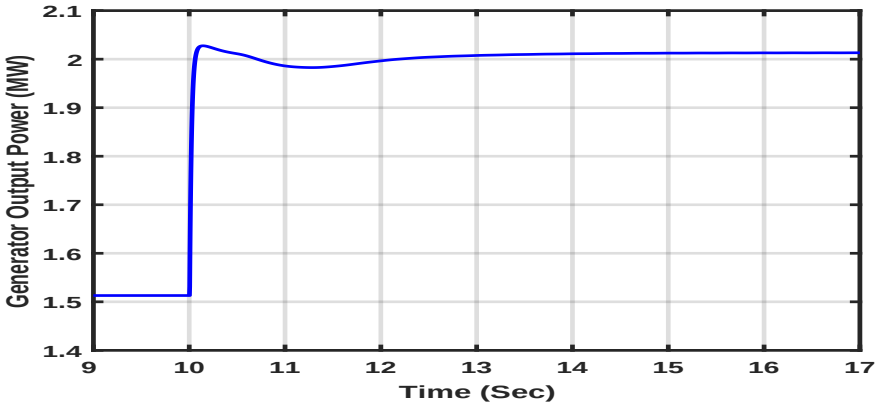

Figure 4.2: Increase in output of the diesel-generator remaining online

In fact, it is the 'speed-droop' governor which responds to the frequency excursion by changing the gate position of the fuel valve. When the generation needs to be increased, the 'speed-droop' governor arranges more fuel intake to the engine and, by doing that, it increases the mechanical torque input which is then translated to increased electrical output power from the synchronous generator.

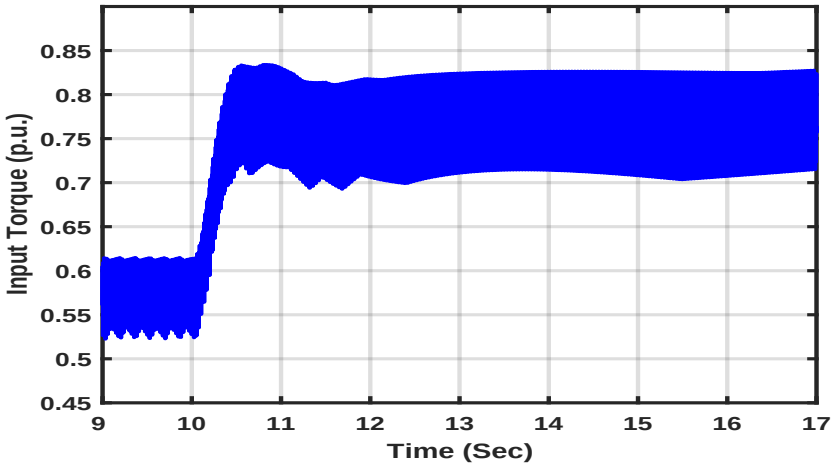

Figure 4.3: Increase in mechanical input torque to the generator

Certainly, at the very beginning of the disturbance the kinetic energy stored in the rotor is released, thus providing inertial response. The inertia constant has been set at 1.65 second for each one of the generators so, contribution to the inertial response is also the same from each of them. Inertial response tries to arrest the rate of change in frequency which affects the lowest frequency point as well.

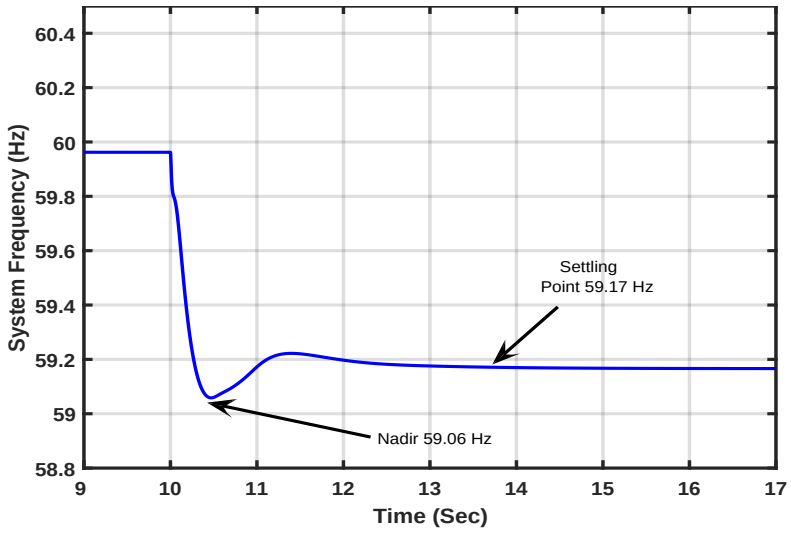

Figure 4.4: System frequency in all-synchronous generator system

In this case, the frequency nadir occurs at 59.06 Hz. As the lost generation is supplemented by the increased generation from the remaining generators, the system frequency settles to some point (59.17 Hz) and gets stabilized. But it doesn't go back to its nominal level, just as it was before the disturbance. A constant error (Δf) still remains, which can be corrected by the secondary frequency response or automatic generation control (AGC) but, that is beyond the scope of this work.

4.2.2 Study Case II

For study case II, the system is designed in such a way so that, it yields similar frequency response to the all synchronous generator based system in times of system fault. However, the model is not void of synchronous generator and has two conventional diesel generators, each one rated at 2 MW and is operating at 1.5 MW. A PV plant that produces real power around 6 MW is also included . As an equivalent electrical circuit based on a controllable current source is representing the PV plant , the irradiance and input temperature are assumed to be constant. A BESS rated at 4 MW is another component of the proposed system. A linear load rated at 6 MW is connected to the system akin to case I.

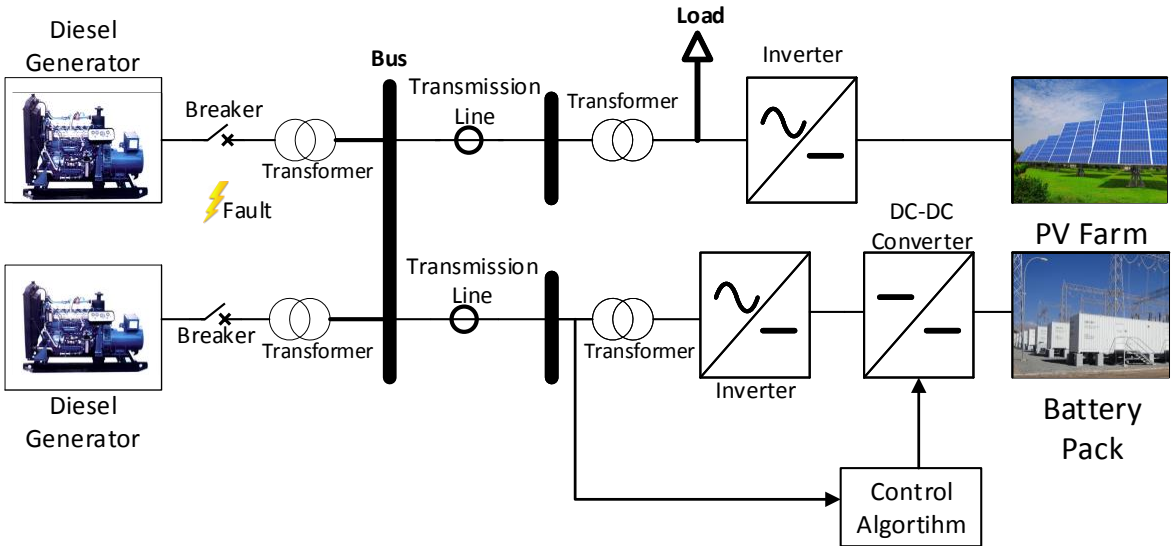

Figure 4.5: Layout of the microgrid with BESS and PV plant.

The BESS is being charged during the simulation, and the goal is to extract droop response from BESS during charging. Before the disturbance takes place the BESS is being charged at a constant pre-set current which is then reduced as per the droop control algorithm which finds the amount of current supposed to be deducted from the pre-set value from the real power calculated from the following equation:

$$P_{BESS} = K_p(f_{ref} - f) \tag{4.1}$$

After one of the two generators gets tripped, the other one raises its output to replenish the lost generation. Here, the generator raises its operating point from 1.5MW to almost 2MW implying that it uses its capacity to its fullest extent.

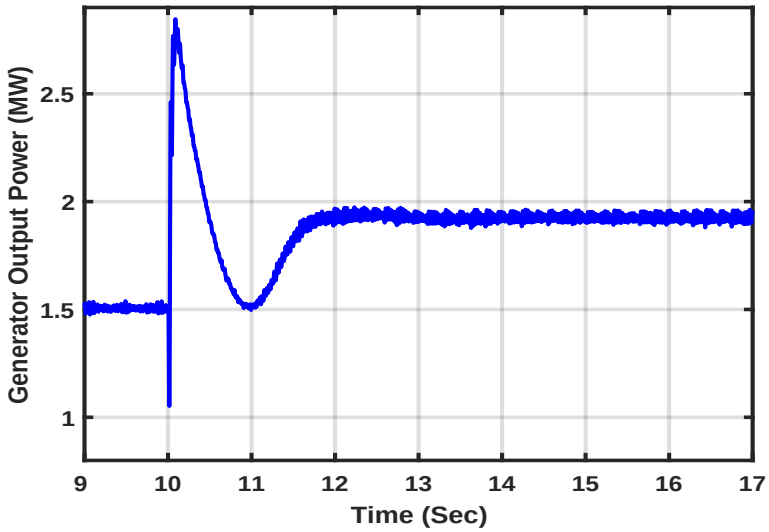

Figure 4.6: Increase in output of the diesel-generator remaining online in case II

The BESS here has been set to provide 5% droop, so its consumption also changes accordingly. The BESS acts as a smart load whose consumption can be manipulated as per the need. Here, the consumption has been reduced from around 3 MW to 1.9 MW.

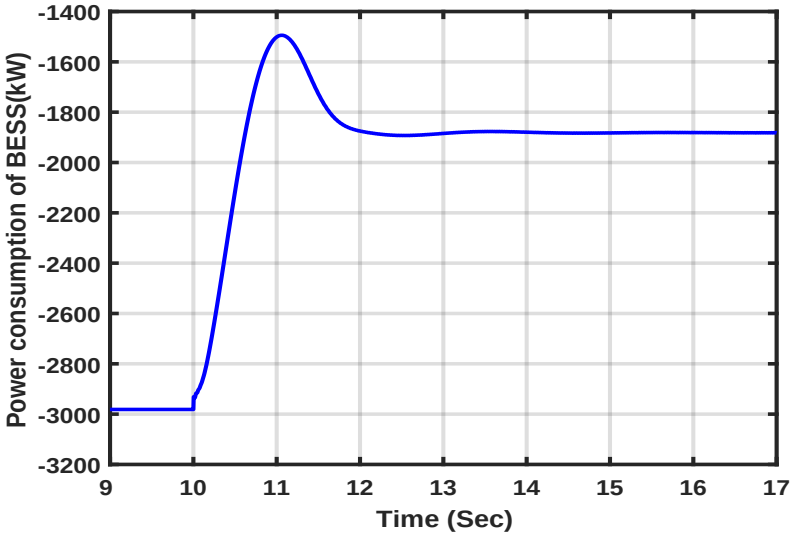

Figure 4.7: Reduction in BESS power consumption for providing droop response

Reduction in the BESS consumption is the result of the reduction of BESS charging current controlled as per the droop control algorithm. The battery terminal voltage changes very insignificantly that's why it has

minimal effect on the change in power consumption.

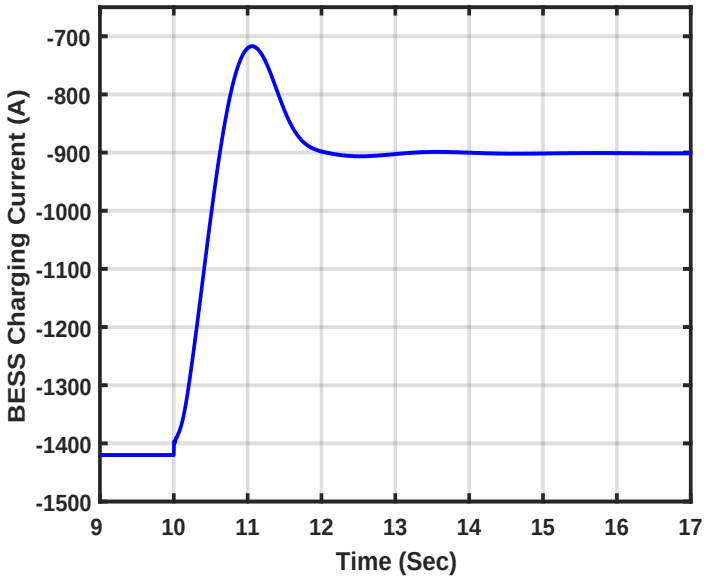

Figure 4.8: Reduction in BESS charging current with droop control activated

The battery charging current has been reduced from 1420 A to 900 A in this case. The effect of this change in power consumption is visible from the look at system's frequency response. Now, the system frequency settles at 59.19 Hz which is very close to the all-synchronous generator system. The nadir takes place at 58.90 Hz; so, it is obvious that the final settling frequency does depend on the droop response whereas the nadir doesn't depend on it too much.

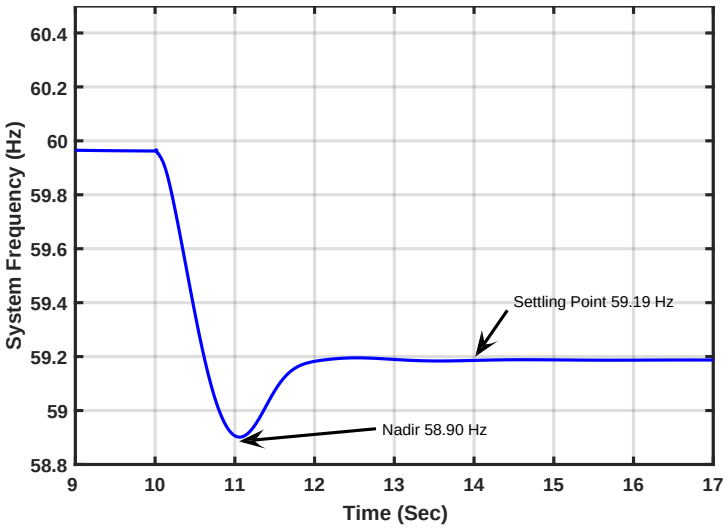

Figure 4.9: System frequency with droop control

4.2.3 Study Case III

The system set-up for study case III is just similar to case II but, there are some modifications introduced in the charging current control algorithm. Here, the amount of power consumption to be shed takes inertial effect into account. So, the amount of charging current to be reduced is found from the power supposed to be obtained from the following equation,

$$P_{BESS} = K_d \frac{df}{dt} + K_p(f_{ref} - f) \tag{4.2}$$

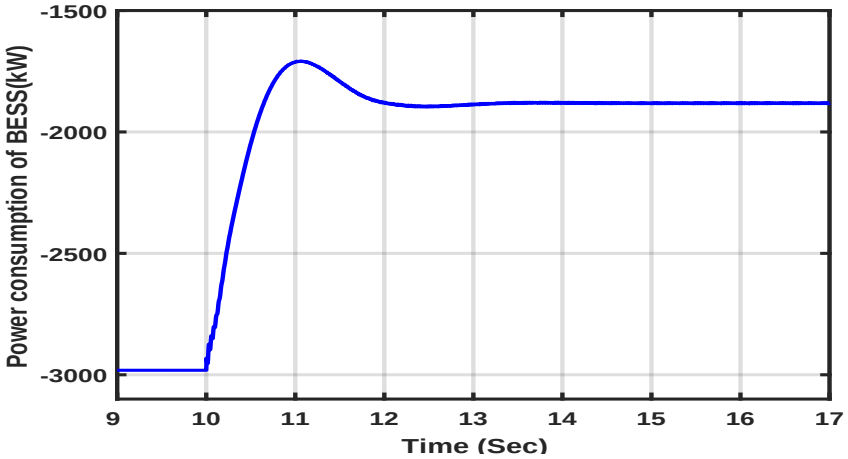

Figure 4.10: Reduction in BESS power consumption for providing droop & IR response

Comparing the power consumption by BESS in case II and case III, it can be concluded that at steady state the power consumptions are same, but the minimum consumption varies. Case II has less consumption than case III. The reason lies in the difference in frequency nadirs.

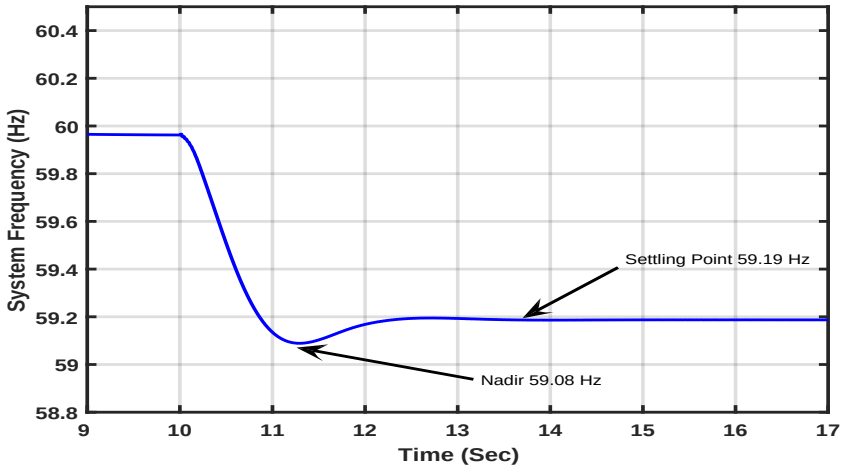

Figure 4.11: System frequency with droop & inertia response activated

It is clear from the above figure that the frequency nadir in case II is lower than the nadir at case III. It results in a higher amount of power shedding request. Though the inertial term adds some more power shedding request, it is largely overwhelmed by the droop portion of the equation. Naturally, just like the BESS power consumption, the charging current will have a higher magnitude at the minimum point than case II.

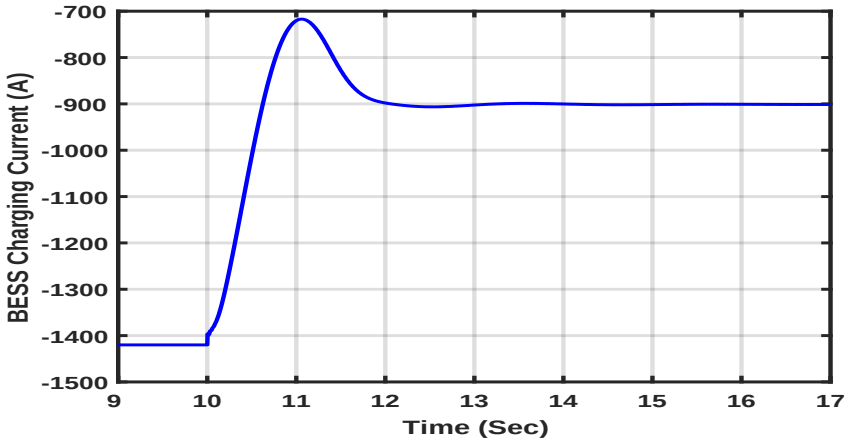

Figure 4.12: Reduction in BESS charging current with droop control activated

Due to the incorporation of inertial response as it tries to arrest the ROCOF more than that of the case without IR, changes in the rate of decrease in frequency has been slowed down in case III compared to that in case II. Slower ROCOF affects the frequency nadir too as a consequence. Here, the frequency nadir has been improved by the IR whereas the settling point remains the same. So, it can be concluded that the frequency nadir depends on IR to some extent.

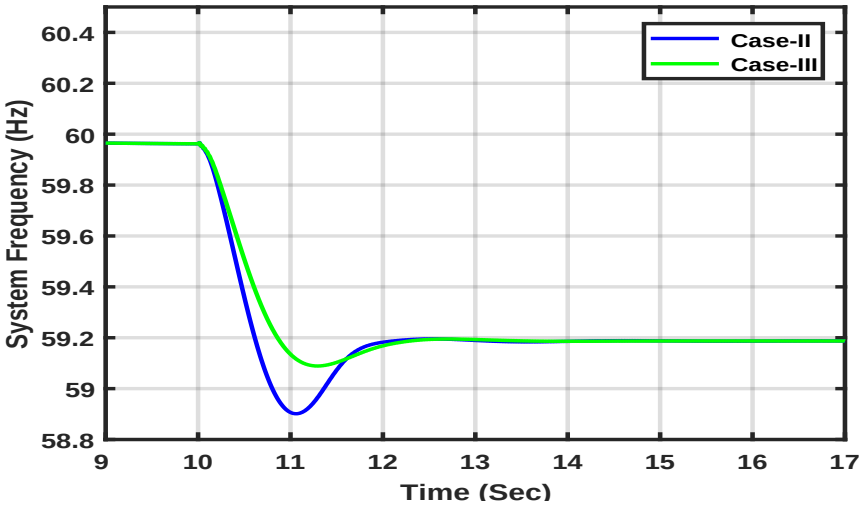

Figure 4.13: Comparison of system frequency's rate of change between case II & III

One thing worthy of looking at in the frequency plot of case III is that, when both droop and inertial response algorithm have been activated, there is less oscillation in the frequency curve. It implies that the damping effect is higher here compared to case II and the system frequency also seems to settle faster than the previous cases.Overall, it can be concluded that system frequency response when both inertial and droop response algorithms are activated look similar to that of in all-synchronous generator case. It produces the almost the same frequency nadir (59.08 Hz) and same frequency settling point (59.19 Hz). So, BESS can successfully emulate the role of the synchronous machine in providing inertial and droop response services. To implement the IR, it is required to find the ROCOF. Here, to perform that work, the derivative block from PSCAD library has been used. Unfortunately, the derivative block is prone to noise, and it has some time delay problem which introduces a time-lag in response.

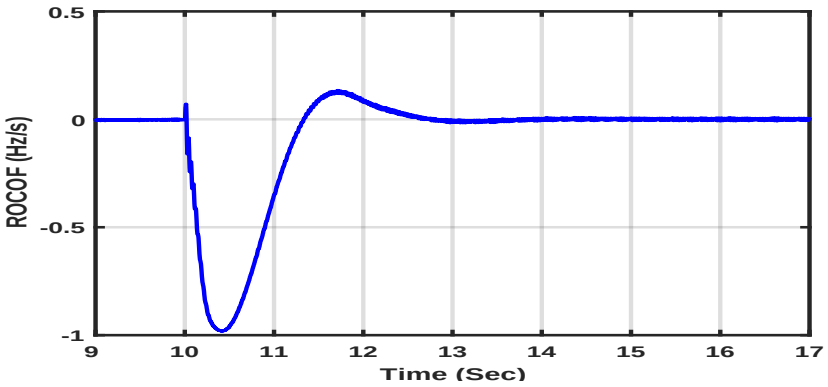

Figure 4.14: System Frequency derivative in case III

4.2.4 Study Case IV

In study case III, the IR algorithm remains in action from the beginning of the disturbance to the steady state. This is kind of contradictory to the traditional practice in the conventional power system. Referring to figure 2.1, it is evident that inertial response service should stop when system frequency hits its nadir. Following figure denotes the boundary where IR should be active.

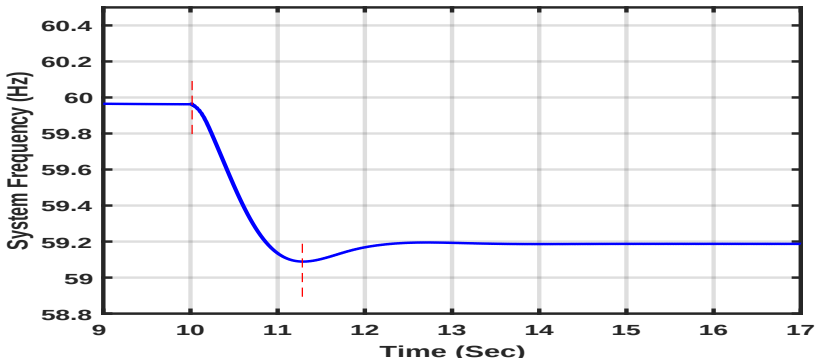

Figure 4.15: System frequency region where IR should be active

To the knowledge of the author, there is not a single literature that has addressed the issue carefully. Most of the work addressing to get IR services from energy storage devices have made IR activated until the frequency reaches its steady state. Though not very significant in terms of the amount of real power, it is still a wastage of the controller and when frequency gets past the nadir, it affects the whole frequency response negatively as the ROCOF becomes positive for a short while.

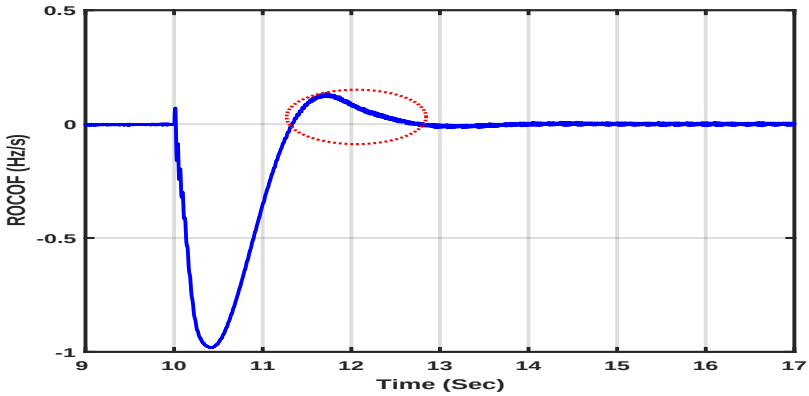

Figure 4.16: System Frequency derivative in case III with positive portion highlighted

In this study case, the operation of IR has been restricted between the beginning of the system disturbance and the frequency nadir. It has been accomplished by forcing the output of the IR algorithm to become zero, once the value ROCOF becomes positive. The modified ROCOF will now look like the following.

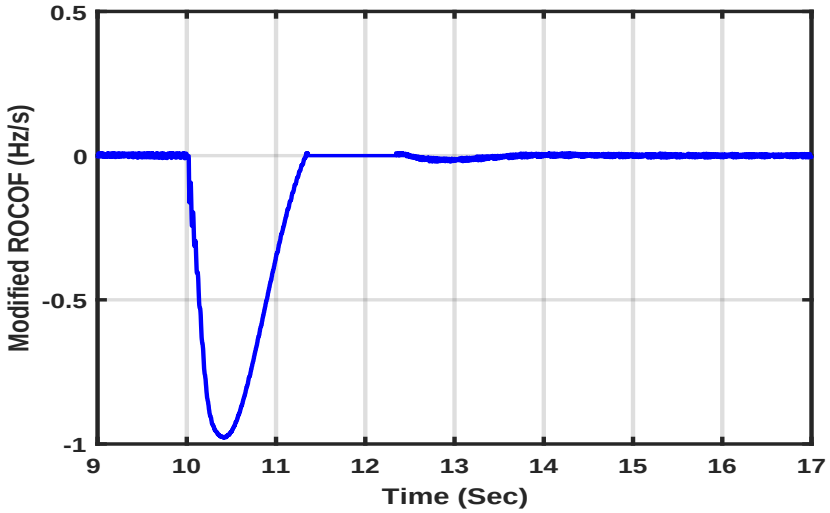

Figure 4.17: System Frequency derivative in case IV

Due to the absence of the negatively affecting inertial effect insignificant changes have been found in BESS charging current and in its consumption.

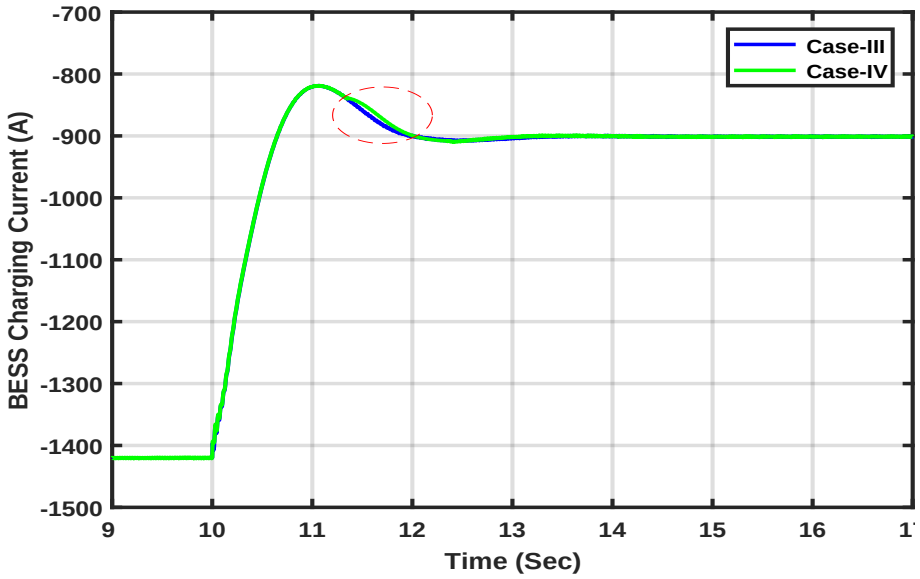

Figure 4.18: Change in BESS charging current due to modified ROCOF

Consequently, a little change is also visible on system frequency response.

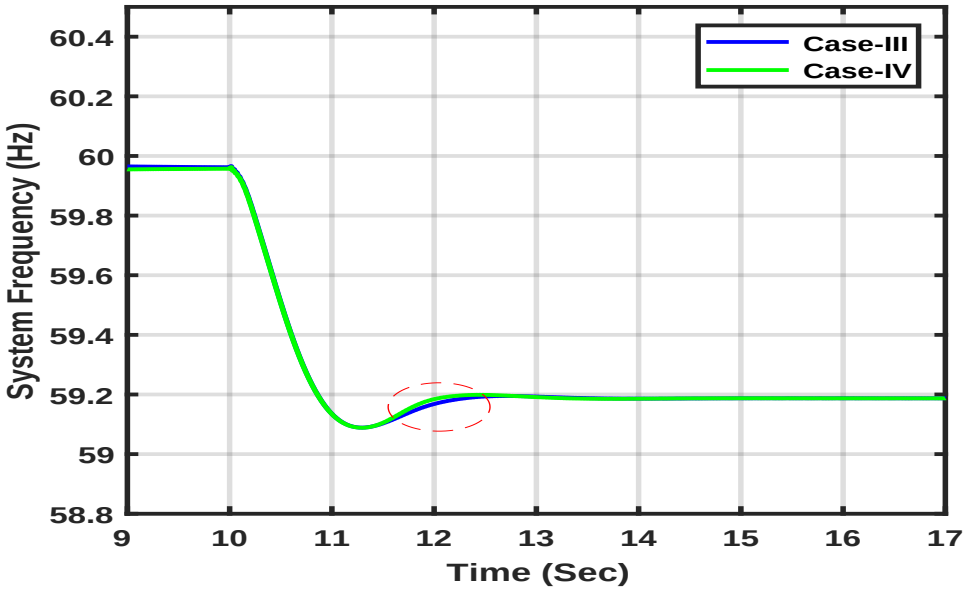

Figure 4.19: Change in system frequency due to modified ROCOF

One of the major advantage of the proposed method is that while supporting this frequency support service to the system the BESS can still continue to be charged which is represented by the consistent rise in SOC

of the battery pack with insignificant difference among themselves.

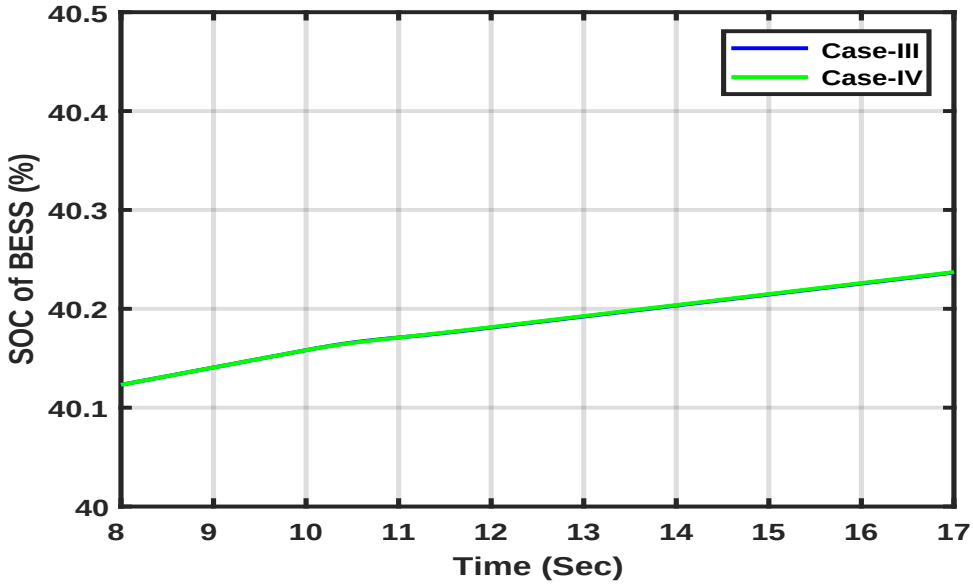

Figure 4.20: Consistent rise in SOC

An overall comparison among several parameters from study case I, II and III, is shown in the table below.

Case No.	Study Case	Frequency Nadir[Hz]	Settling Point[Hz]	Settling Time[s]
I	Without BESS	59.06	59.17	3.10
II	With BESS(only droop)	58.90	59.19	3.92
III	With BESS (with IR)	59.08	59.19	2.76

Table 4.1: Frequency response of study cases, performance indices

4.3 Justification of the Comparison

The work is claiming that the basis of comparison that has been made among study cases is justified. This is because the generation load similarity (not according to the type). In case I, four diesel generators each one operating at 1.5 MW is providing a 6 MW linear load. When one of them is tripped, the remaining three raises their output to almost 2 MW to support the load.

In both study case II and III, two diesel generators operating at 1.5 MW are present. A 6 MW PV power generating plant is connected to the microgrid along with a 6 MW linear load. So, it can be assumed that the PV plant is feeding the load fully of its own. A BESS rated at 4 MW but set to consume 3 MW initially has been included in the system seemingly gets its supply from the generators. When one of the generators is tripped a 1.5 MW generation has been dropped which is similar to case I, where the total rated power

of the remaining generator was 6 MW, and here the rating of the remaining generator is 2 MW, and the battery has a rating 4 MW so, in total, it is 6 MW. The BESS rating is just twice of a single diesel generator so, in total this equivalent system has three similar generators remaining after the trip. The droop response that is expected from the BESS is to provide 5% droop and inertial response based on inertia constant, 1.65 second just like any other synchronous generator in the system. So, this 6 MW should emulate the similar droop and inertial response as in case I. PV plant here is just playing neutral when the question of droop or inertial response comes in. So, the system has been prepared to study the effect of droop and inertial response from BESS and the remaining generator. And from the results that have been achieved so far, it can be concluded that the BESS with the proposed algorithm has been able to do that.

Chapter 5

Conclusion and Future Work

5.1 Conclusion

The growing deployment of environment-friendly energy sources doesn't come without their shortcomings. From the system security perspective, they raise a serious question to the system operators that, how they will cope up with this changing trend. More power electronics interfaced energy sources mean less system inertia and less control over system frequency when the equilibrium between generation and demand is lost. This work has tried to resort to some already existing system components to address the issue . BESSs are in use for providing many grid support services for a long time, so the technology is pretty much well established. In addition to that, recently the cost of battery has gone down significantly which is another driving force why BESS has been chosen for short-term ancillary support services. Moreover, this work is kind of exceptional from the role of BESS. It provides the frequency response while in charging mode which is quite against the stream. So, it can be assumed that during the daytime when there is surplus energy, the BESS will act as a storing device and simultaneously it can provide frequency support service. At night time, it can provide power to the grid thus making it quite useful all day around and pretty feasible from an economic point of view.

A comprehensive literature review has been accomplished to better understand what available approaches are out there to address the issue. Based on the review of available technologies and after having compromised with the shortcomings a solution approach has been adopted that is to make BESS perform as a VSG to provide IR and droop response at its charging stage. A brief overview of various frequency support services has also been done to give some insight how the conventional synchronous machine based system tackles its frequency events. The choice for Li-ion battery as the central part of the BESS has been rationalized by making a comparison with its other counterparts.

PSCAD has been used as a modeling tool for the microgrid components. It can solve electromagnetic and electro-mechanical system equations which is especially required in this case as the frequency events comprise both electromagnetic and electro-mechanical response. As a part of modeling the diesel generator, the design of governor, diesel engine, and synchronous generator have been performed with having considered many details. A 'speed-droop' type governor has been chosen to control the fuel intake to the diesel engine in response to the frequency excursions. The synchronous generator model has been customized to suit the

need of this work.
Voltage source converters (VSCs) have been used to interface the dc systems to the microgrid. The dc-link voltage control and direct and quadrature axis current control have been modified to produce the desired performance. LCL filter parameters which are highly important component to get rid of switching harmonics have been designed for handling expected higher power (higher voltage and current) exchange between the ac-side and the dc-side.
A PV plant is represented with an equivalent electrical circuit with a controllable current source. It is performing as a constant power generating unit in this case without making any contribution to the system's frequency event. A buck-boost converter has been introduced as a part of the two-stage control on power exchange. As the focus is mainly on the charging stage, only the buck mode operation of the dc-dc converter has been demonstrated. The principal control over battery charging is accomplished with the buck-converter so, major modification has been done to its current control algorithm. The swing equation has been incorporated into the charging current control algorithm to determine how much power should be shed to provide inertial and droop response. For battery charging constant current(CC) charging scheme has been adopted.
To test the efficacy of the proposed algorithm, four cases have been studied. To compare the performance an all-synchronous machine based grid has been set-up and simulated. The inertial and droop response, in this case, are all contributed by the conventional diesel generators. Another model has been prepared with a reduced number of diesel generators. A PV plant and BESS has been incorporated in that model to implement and test the performance of the proposed algorithm. In one case the system's frequency profile is observed with only droop response algorithm activated and in another case with both droop and inertial response activated. With both services activated, the system frequency looks almost similar to the all synchronous generator case. A fourth case has been proposed to utilize the inertial controller as per the traditional practice where the inertial response portion is not allowed to effect the system performance negatively.
The proposed approach in this work provides food to the thought of utilizing the potential of BESS even when it is being charged. This utilization can be broadened in many ways to ensure a resilient energy solution.

5.2 Future Work

There are many places where the current work can be improved, or the concept can be used to solve other related problems. Some of the areas where improvements can be brought in are as follows:

- Only inertial response and droop response service have been focused in current work. Potential of BESS may be sought for providing other frequency support services like AGC or tertiary frequency response.
- Performance of the proposed concept can be tested in total synchronous machine free system.
- Active loads like induction motors can be tested to provide these short-term ancillary services.
- Optimization techniques can be adopted to find the optimal size of the BESS and the microgrid components.

- Dynamic tuning of the current controller can be experimented to reduce the utilization of the controllers.
- Non-linear devices like PLLs can be replaced with more reliable phase detection system which will reduce the oscillation during the synchronization of dc systems with the rest of the grid.
- More realistic battery model can be used to determine how things may happen in real world.
- Instead of using linear loads, non-linear loads can be introduced to see their effect on system's performance.
- Over-frequency event can be studied to prove the ubiquitous utility of the algorithm.
- Dynamic control method like i-droop control[82] can be tested to see its potential against the proposed one.
- As the control algorithm is only dependent on local frequency measurement, the scope can be broadened by finding a more effective way that can be also effective in the multi-area system.

Appendix

PSCAD GUI Models

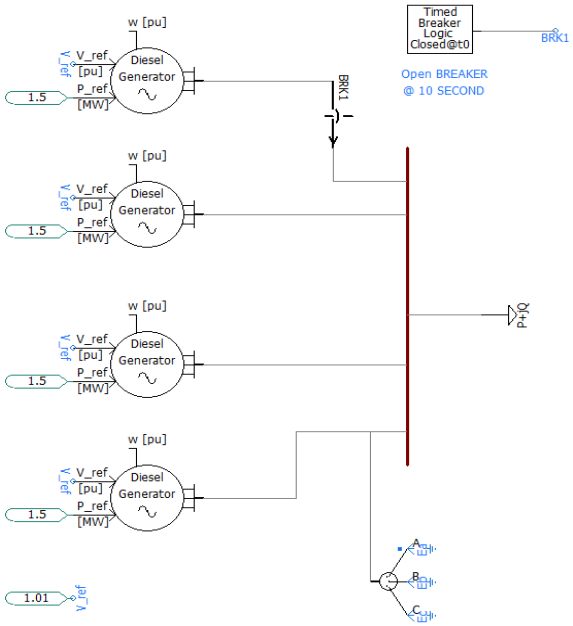

Figure A1: PSCAD GUI model for study case I: all-synchronous machine system

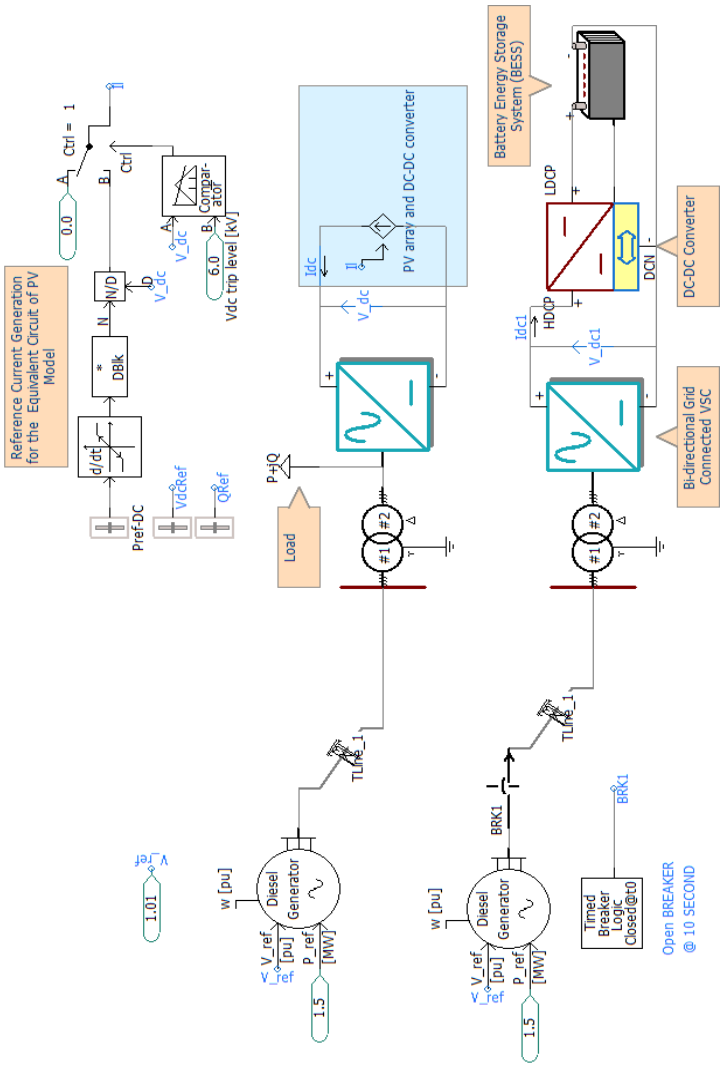

Figure A2: PSCAD GUI model for study case II, III and IV

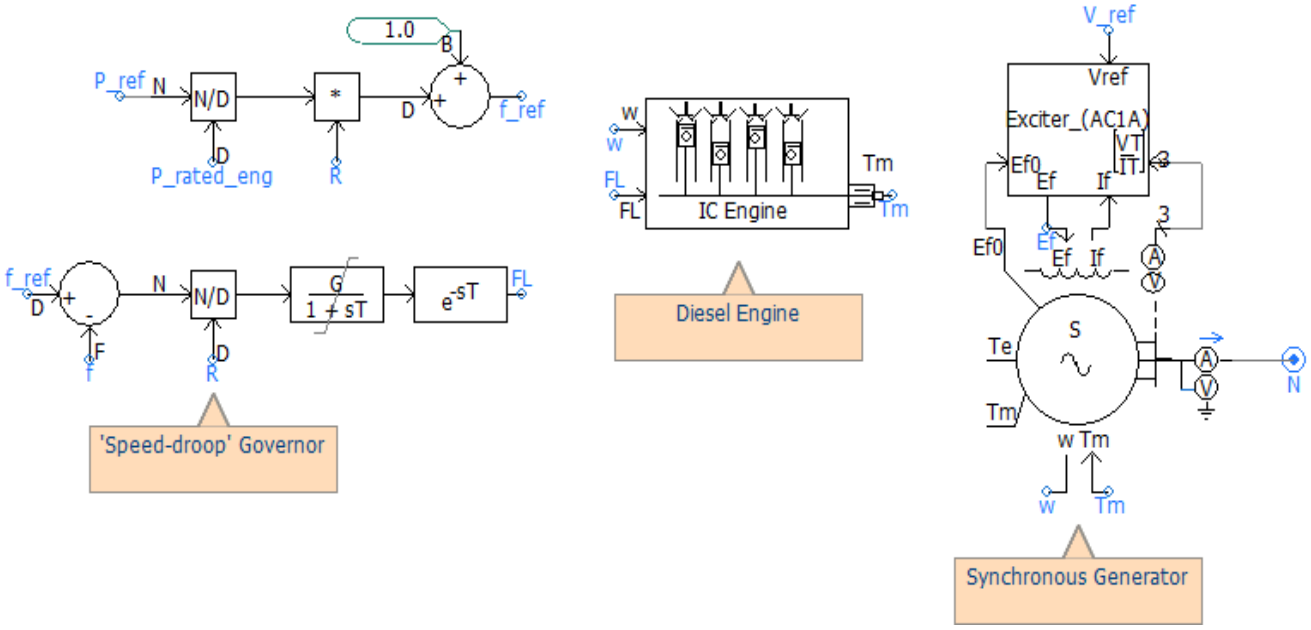

Figure A.3: Diesel generator set

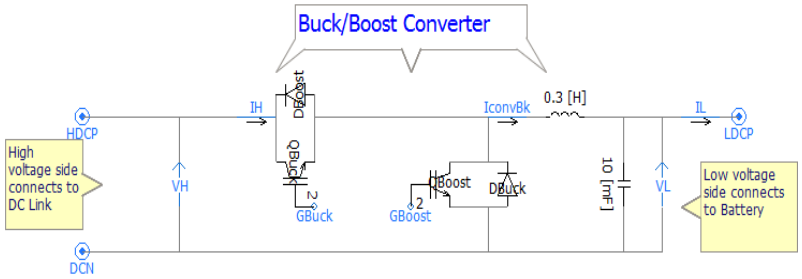

Figure A.4: Buck-Boost converter

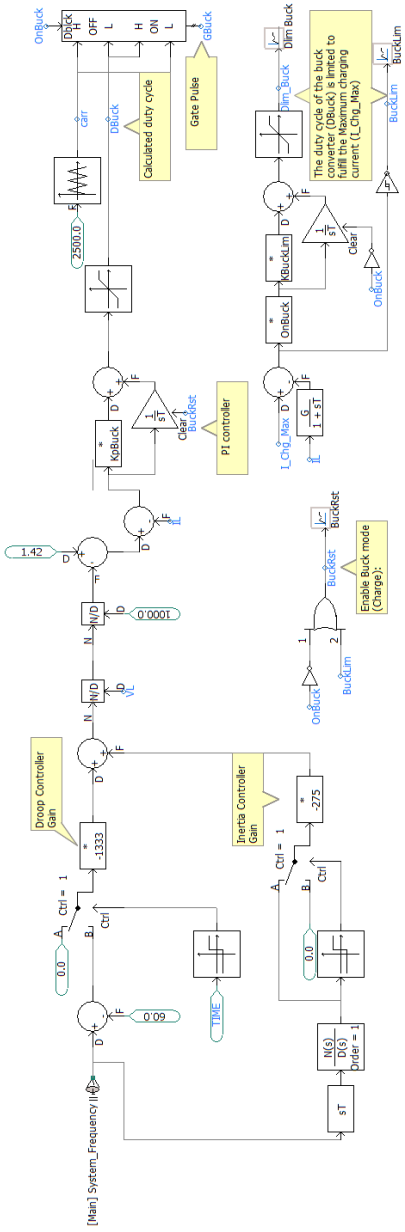

Figure A.5: BESS charging current controller

Bibliography

[1] BP Energy Outlook, BP LLC, 2018, pp. 6-7.

[2] Renewables 2016, Global Status Report, Paris: Renewable Energy Policy Network for the 21st Century, 2016, p. 158.

[3] Global Trends in Renewable Energy Investment 2018, UN Environment's Economy Division, Frankfurt:Frankfurt School-UNEP Collaborating Centre for Climate Sustainable Energy Finance, and Bloomberg New Energy Finance, 2018.

[4] D. Ing and G. Kramer, 'SUPERCONDUCTIVITY IN ENERGY STORAGE', 1995, p. 44.

[5] Y. V. Makarov, S. Lu, M. Jian and T.-B. Nguyen, 'Assessing the value of regulation resources based on their time response characteristics', Pacific Northwest National Lab. (PNNL), Richland, 2008.

[6] K. Vu, R. Masiello and R. Fioravanti, 'Benefits of fast-response storage devices for system regulation in ISO markets', in *Power and Energy Society General Meeting*, 2009, pp. 1-8.

[7] M. Motyka, 2018 outlook on renewable energy, My take: Marlene Motyka ,NY: Deloitte Center for Energy Solution, 2018, p. 6.

[8] Technical Specification-Three Phase Battery System. Winnipeg: Manitoba HVDC Research Center, 2017, p. 2.

[9] M. Torres and L. AC. Lopes, 'Virtual synchronous generator: A control strategy to improve dynamic frequency control in autonomous power systems', *Energy and Power Engineering*, vol. 05, no. 02, p. 32, 2013.

[10] A. Buckspan, J. Aho, P. Fleming, Y. Jeong, and L. Pao, 'Combining droop curve concepts with control systems for wind turbine active power control', in *Power Electronics and Machines in Wind Applications (PEMWA)*, 2012, pp. 1-8.

[11] M. Altin, R. Teodorescu, B. Jensen, U. Annakkage, F. Iov, and P. Kjr, 'Methodology for assessment of inertial response from wind power plants', in *Power and Energy Society General Meeting*, 2012, pp. 1-8.

[12] G. C. Tarnowski, 'Coordinated Frequency Control of Wind Turbines in Power Systems with High Wind Power Penetration', Technical University of Denmark, 2011.

[13] J. Machowski, J. Bialek, and J. Bumby, *Power system dynamics: stability and control*. Wiley, 2008.

[14] V. Gevorgian, Y. Zhang and E. Ela, 'Investigating the impacts of wind generation participation in interconnection frequency response', *IEEE Transactions on Sustainable Energy*, vol. 06, no. 03, 2015, pp. 1004-1012.

[15] S. Sharma, S. -H. Huang and NDR. Sarma, 'System inertial frequency response estimation and impact of renewable resources in ERCOT interconnection', in *Power and Energy Society General Meeting*, 2011, pp. 1-6.

[16] G. C. Tarnowski, P. C. Kjar, P. E. Sorensen and J. Ostergaard, 'Variable speed wind turbines capability for temporary over-production', in *Power and Energy Society General Meeting*, 2009, pp. 1-7.

[17] P. Tielens and D. Hertem, 'The Relevance of Inertia in Power System', *Renewable and Sustainable Energy Reviews*, vol. 55, 2015, pp. 999-1009.

[18] J. M. Guerrero, L. G. De vicuña, J. Matas, M. Castilla and J. Miret, 'Output impedance design of parallel-connected UPS inverters with wireless load-sharing control', *IEEE Transactions on Industrial Electronics*, vol. 52, no. 04, 2005, pp. 1126-1135.

[19] K. De Brabandere, B. Bolsens, J. Van den Keybus, A. Woyte, J. Driesen and R. Belmans, 'A voltage and frequency droop control method for parallel inverters', *IEEE Transactions on Power Electronics* ,vol. 22, no. 04, 2007, pp. 1107-1115.

[20] J. M. Guerrero, L. Hang and J. Uceda, 'Control of distributed uninterruptible power supply systems', *IEEE Transactions on Industrial Electronics*, vol. 55, no. 08, 2008, pp. 2845-2859.

[21] Q.-C. Zhong and Y. Zeng, 'Can the output impedance of an inverter be designed capacitive?', in *37th Annual Conference on IEEE Industrial Electronics Society, IECON 2011*, 2011, pp. 1220-1225.

[22] Y. G. Rebours, D. S. Kirschen, M. Trotignon and S. Rossignol, 'A survey of frequency and voltage control ancillary servicesPart I: Technical features', *IEEE Transactions on power systems*, vol. 22, no. 01, 2007, pp. 350-357.

[23] N. Cohn, *Control of Generation and Power Flow on Interconnected Systems*, NY: Wiley, 1971.

[24] G. Delille, B. Francois and G. Malarange, 'Dynamic frequency control support: A virtual inertia provided by distributed energy storage to isolated power systems', in *Innovative Smart Grid Technologies Conference Europe (ISGT Europe)*, 2010, pp. 1-8.

[25] J. Morren, S. WH. De Haan, W. L. Kling and JA. Ferreira, 'Wind turbines emulating inertia and supporting primary frequency control', *IEEE Transactions on Power Systems*, vol. 21, no. 01, 2006, pp. 433-434.

[26] J. Zhang, 'Research on flywheel energy storage system using in power network', in *International Conference on Power Electronics and Drives Systems (PEDS)*, 2005, pp. 1344-1347.

[27] S. Padrón, JF. Medina and A. Rodríguez, 'Analysis of a pumped storage system to increase the penetration level of renewable energy in isolated power systems. Gran Canaria: a case study', *Energy*, vol. 36, no. 12, 2011, pp. 6753-6762.

[28] J. Zhu, C. D. Booth, G. P. Adam, A. J. Roscoe and C. G. Bright, 'Inertia emulation control strategy for VSC-HVDC transmission systems', *IEEE Transactions on Power Systems*, vol. 28, no. 02, 2013, pp. 1277-1287.

[29] M. Albu, A. Nechifor and D. Creanga, 'Smart storage for active distribution networks estimation and measurement solutions', in *Instrumentation and Measurement Technology Conference (I2MTC)*, 2010, pp. 1486-1491.

[30] YT. Tan, 'Impact on the power system with large penetration of photovoltaic generation', The University of Manchester Institute of Science and Technology, 2004.

[31] Y. Liu, L. Zhu, L. Zhan, J. R. Gracia, T. King Jr. and Y. Liu, 'Active power control of solar PV generation for large interconnection frequency regulation and oscillation damping', *International Journal of Energy Research*, vol. 40, no. 03, 2016, pp. 353-361.

[32] PP. Zarina, S. Mishra and PC. Sekhar, 'Exploring frequency control capability of a PV system in a hybrid PV-rotating machine-without storage system', *International Journal of Electrical Power and Energy Systems*, vol. 60, 2014, pp. 258-267.

[33] E. Muljadi, V. Gevorgian, M. Singh and S. Santoso, *Understanding inertial and frequency response of wind power plants*, IEEE, 2012.

[34] Y. Zheng, 'Virtual Inertia Emulation in Islanded Microgrids with Energy Storage System', TU Delft, 2016.

[35] L. Zeni, A. J. Rudolph, J. Münster-Swendsen, I. Margaris, A. D. Hansen and P. Sørensen, 'Virtual inertia for variable speed wind turbines', *Wind Energy*, vol. 16, no. 08, 2013, pp. 1225-1239.

[36] I. Serban and C. Marinescu, 'Control strategy of three-phase battery energy storage systems for frequency support in microgrids and with uninterrupted supply of local loads', *IEEE Transactions on Power Electronics*, vol. 29, no. 09, 2014, pp. 5010-5020.

[37] A. Vassilakis, P. kotsampopoulos, N. Hatziargyriou and V. Karapanos, 'A battery energy storage based virtual synchronous generator', in *Bulk Power System Dynamics and Control-IX Optimization, Security and Control of the Emerging Power Grid (IREP), 2013 IREP Symposium*, 2013, pp. 1-6.

[38] V. Knap, R. Sinha, M. Swierczynski, D.-I. Stroe and S. Chaudhary, 'Grid inertial response with lithium-ion battery energy storage systems', in *IEEE 23rd International Symposium on Industrial Electronics (ISIE), 2014* , 2014, pp. 1817-1822.

[39] F. Gonzalez-Longatt, and S.M. Alhejaj, 'Enabling inertial response in utility-scale battery energy storage system', in *IEEE 2016 Innovative Smart Grid Technologies, Asia (ISGT-Asia)*, 2016, pp. 605-610.

[40] H.-P. Beck and R. Hesse, 'Virtual synchronous machine', in *9th International Conference on Electrical Power Quality and Utilisation (EPQU)*, 2007, pp. 1-6.

[41] Q.-C. Zhong and G. Weiss, 'Synchronverters: Inverters that mimic synchronous generators', *IEEE Transactions on Industrial Electronics*, vol. 58, no. 04, 2011, pp. 1259-1267.

[42] T. V. Van, K. Visscher, J. Diaz, V. Karapanos, A. Woyte, M. Albu, J. Bozelie, L. Tom and D. Federenciuc, 'Virtual synchronous generator: An element of future grids', in *Innovative Smart Grid Technologies Conference Europe (ISGT Europe)*, 2010, pp. 1-7.

[43] J. Driesen and K. Visscher, 'Virtual synchronous generators', in *Power and Energy Society General Meeting*, 2008, pp. 20-24.

[44] Y. Chen, R. Hesse, D. Turschner and H.-P. Beck, 'Improving the grid power quality using virtual synchronous machines', in *International Conference on Power Engineering, Energy and Electrical Drives (POWERENG)*, 2011, pp. 1-6.

[45] K. Sakimoto, Y. Miura and T. Ise, 'Stabilization of a power system with a distributed generator by a virtual synchronous generator function', in *IEEE 8th International Conference on Power Electronics and ECCE Asia (ICPE & ECCE)*, 2011, pp. 1498-1505.

[46] Y. Hirase, K. Abe, K. Sugimoto and Y. Shindo, 'A grid-connected inverter with virtual synchronous generator model of algebraic type',*Electrical Engineering in Japan*, vol. 184, no. 04, 2013, pp. 10-21.

[47] P. Krause, O. Wasynczuk and S. Sudhoff, *Analysis of electric machinery and drive systems*, Wiley, 2002, pp. 200-208.

[48] P. Anderson and A. Fouad, *Power system control and stability*, IEEE Press, 1994, pp. 83-94.

[49] I. Hadjipaschalis, A. Poullikkas and V. Efthimiou, 'Overview of current and future energy storage technologies for electric power applications', *Renewable and Sustainable Energy Reviews*, vol. 13, no. 6-7, 2009, pp. 1513-1522.

[50] www.energystorageexchange.org, 'Gloabal Project Installations Over Time'. [Online]. Available:`http://www.energystorageexchange.org/projects/data_visualization`.[Accessed: 04-13-2018]

[51] S. M. Lukic, S. G. Wirasingha, F. Rodriquez, J. Cao and A. Emadi, 'Power management of an ultracapacitor/battery hybrid energy storage system in an HEV', in *Vehicle Power and Propulsion Conference (VPPC'06)*, 2006, pp. 1-6.

[52] G. Delile, 'Contribution of Storage to Advanced Management of Electrical Systems: Organizational and Technico-Economics in the Distribution Grids',Central School of Lille,2011.

[53] E. Konstantinos and D. Despoina, '1.5a-Report on Use of Energy Storage Units', DISPOWER, 2003.

[54] F. R. Kalhammer, B. M. Kopf, D. H. Swan, V. P. Roan and, M. P. Walsh, 'Status and Prospects for Zero Emissions Vehicle Technology',Air Resources Board, Sacramento, CA ,2007.

[55] 'Investigation on Storage Technologies for Intermittent Renewable Energies : Evaluation and recommended RD strategy', 2002-2004.

[56] G. Sarre, 'Advanced PV Energy Storage System with Lithium-Ion Batteries', Gelsenkirchen, Germany, 2006.

[57] B. Dunn, H. Kamath and J.-M. Tarascon, 'Electrical Energy Storage for the Grid: A Battery of Choices', *Science*, vol. 334, no. 6058, 2011, pp. 928-935.

[58] www.batteryuniversity.com, 'How Do Lithium Batteries Work?',2011. [Online]. Available: `http://batteryuniversity.com/learn/article/lithium_based_batteries`. [Accessed: 04-19-2018]

[59] V. Etacheri, R. Marom, R. Elazari, G. Salitra and D. Aurbach, 'Challenges in the development of advanced Li-ion batteries: a review', *Energy & Environmental Science*, vol. 04, no. 09, 2011, pp. 3243-3262.

[60] V. Friedel,'MODELING AND SIMULATION OF A HYBRID WIND-DIESEL MICROGRID',Royal Institute of Technology (KTH),2009.

[61] H.-D. Lee and, S.-K. Sul,'Diesel engine ripple torque minimization for parallel type hybrid electric vehicle',in *IEEE Industry Applications Conference*,Thirty-Second IAS Annual Meeting, IAS 97, 1997, pp. 942-946.

[62] www.cumminsengines.com, 'QSK78 for Mining'. [Online]. Available: `https://cumminsengines.com/qsk78-mining#overview`. [Accessed: 04-23-2018]

[63] P. Kundur, *Power System Stability and Control*, McGraw-Hill, 1994.

[64] 'IEEE Recommended Practice for Excitation System Models for Power System Stability Studies (IEEE Std 421.5 - 2005)', 2006.

[65] P. C. Krause,*Analysis of Electric Machinery and Drive Systems*,IEEE Press,2002.

[66] GN. Kariniotakis and GS. Stavrakakis,'A general simulation algorithm for the accurate assessment of isolated diesel-wind turbines systems interaction. Part II: Implementation of the algorithm and case-studies with induction generators',*IEEE Transactions on Energy Conversion*,vol. 10, no. 03, 1995, pp. 584-590.

[67] C.W. Leung, E. Hy, J. Ge and A. S.-J. Santiago, 'SCE PSCAD Library Component Third Quarter Report', Southern California Edison, 2015.

[68] *PSCAD User's Guide*, v4.6, Manitoba HVDC Research Center,Winnipeg, MB, Canada, April, 2016, pp. 299-314. Accessed on: May 8, 2018. [Online]. Available:`https://hvdc.ca/uploads/knowledge_base/pscad_users_guide_v4_6.pdf?t=1497534232`.

[69] A. Ghoshal and J. Binod, 'A Method To Improve PLL Performance Under Abnormal Grid Conditions', in *National Power Electronic Conferences*,Bangalore, India ,2007.

[70] X. Lu, 'Minimizing DC Capacitor Current Ripple and DC Capacitance Requirement of the HEV Converter/Inverter System',Michigan State University ,2012.

[71] KS. Gopalakrishnan, S. Das and G. Narayanan, 'Analytical expression for RMS DC link capacitor current in a three-level inverter', 2011.

[72] A. Reznik, M. G. Simões, A. Al-Durra and SM. Muyeen, '*LCL* filter design and performance analysis for grid-interconnected systems', *IEEE Transactions on Industry Applications*, vol. 50, no. 02, 2014, pp. 1225-1232.

[73] M. Liserre, F. Blaabjerg and S. Hansen, 'Design and control of an LCL-filter-based three-phase active rectifier', *IEEE Transactions on Industry Applications*, vol. 41, no. 05, 2005, pp. 1281-1291.

[74] Y. Patel, D. Pixler and A. Nasiri, 'Analysis and design of TRAP and LCL filters for active switching converters', in *IEEE International Symposium on Industrial Electronics (ISIE)*, 2010, pp. 638-643.

[75] T. CY. Wang, Z. Ye, G. Sinha and X. Yuan, 'Output filter design for a grid-interconnected three-phase inverter', in *IEEE 34th Annual Power Electronics Specialist Conference, PESC'03.* , 2003, pp. 779-784.

[76] R. Beres, X. Wang, F. Blaabjerg, C. L. Bak and M. Liserre, 'A review of passive filters for grid-connected voltage source converters', in *Twenty-Ninth Annual IEEE Applied Power Electronics Conference and Exposition (APEC)*, 2014, pp. 2208-2215.

[77] S. Essakiappan, 'Multilevel Converter Topologies for Utility Scale Solar Photovoltaic Power Systems', Texas AM University, 2014.

[78] JG. Pinto, V. Monteiro, H. Gonçalves and J. L. Afonso, 'Onboard reconfigurable battery charger for electric vehicles with traction-to-auxiliary mode', *IEEE Transactions on Vehicular Technology*, vol. 63, no. 3, 2014, pp. 1104-1116.

[79] C. M. Shepherd, 'Design of primary and secondary cells II. An equation describing battery discharge', *Journal of the Electrochemical Society*, vol. 112, no. 7, 1965, pp. 657-664.

[80] O. Tremblay, L.-A. Dessaint and A. Dekkiche, 'A generic battery model for the dynamic simulation of hybrid electric vehicles', in *IEEE Vehicle Power and Propulsion Conference (VPPC)*, 2007, pp. 284-289.

[81] www.rtds.com, 'Real Time Power System Simulation'. [Online]. Available: `https://www.rtds.com/real-time-power-system-simulation/`. [Accessed: 05-08-2018]

[82] E. Mallada, 'iDroop: A Dynamic Droop controller to decouple power grid's steady-state and dynamic performance', in *IEEE 55th Conference on Decision and Control (CDC)*, 2016, pp. 4957-4964.